LEBANESE AMERICAN UNIVERSITY

Receiver Design for MIMO FSO Communication Systems with photon-counting Detection

by
Rami Issam El Mawla

A thesis submitted in partial fulfillment of the requirements for the degree of Master of Science in Computer Engineering

School of Engineering

May 2019

LAU
الجامعة اللبنانية الأميركية
Lebanese American University

THESIS APPROVAL FORM

Student Name: Rami Issam El Mawla I.D. #: 201103526

Thesis Title: Receiver Design for MIMO FSO Communication Systems with photon-counting Detection

Program: Master of Science

Department: Electrical & Computer Engineering

School: of Engineering

The undersigned certify that they have examined the final electronic copy of this thesis and approved it in Partial Fulfillment of the requirements for the degree of:

Master of Science in the major of Computer and Communication Engineering

Thesis Advisor's Name: Chadi Abou-Rjeily

Signature: [redacted] Date: 15 / 5 / 2019 (Day / Month / Year)

Committee Member's Name: Wissam FAWAZ

Signature: [redacted] Date: 15 / 05 / 2019 (Day / Month / Year)

Committee Member's Name: DANI TANNIR

Signature: [redacted] Date: 15 / 5 / 2019 (Day / Month / Year)

LAU
الجامعة اللبنانية الأميركية
Lebanese American University

THESIS COPYRIGHT RELEASE FORM

LEBANESE AMERICAN UNIVERSITY NON-EXCLUSIVE DISTRIBUTION LICENSE

By signing and submitting this license, you (the author(s) or copyright owner) grants the Lebanese American University (LAU) the non-exclusive right to reproduce, translate (as defined below), and/or distribute your submission (including the abstract) worldwide in print and electronic formats and in any medium, including but not limited to audio or video. You agree that LAU may, without changing the content, translate the submission to any medium or format for the purpose of preservation. You also agree that LAU may keep more than one copy of this submission for purposes of security, backup and preservation. You represent that the submission is your original work, and that you have the right to grant the rights contained in this license. You also represent that your submission does not, to the best of your knowledge, infringe upon anyone's copyright. If the submission contains material for which you do not hold copyright, you represent that you have obtained the unrestricted permission of the copyright owner to grant LAU the rights required by this license, and that such third-party owned material is clearly identified and acknowledged within the text or content of the submission. IF THE SUBMISSION IS BASED UPON WORK THAT HAS BEEN SPONSORED OR SUPPORTED BY AN AGENCY OR ORGANIZATION OTHER THAN LAU, YOU REPRESENT THAT YOU HAVE FULFILLED ANY RIGHT OF REVIEW OR OTHER OBLIGATIONS REQUIRED BY SUCH CONTRACT OR AGREEMENT. LAU will clearly identify your name(s) as the author(s) or owner(s) of the submission, and will not make any alteration, other than as allowed by this license, to your submission.

Name: Rami Issam El Raola

Signature: [redacted]

Date: 17 / 05 / 2019
Day Month Year

LAU
الجامعة اللبنانية الأميركية
Lebanese American University

PLAGIARISM POLICY COMPLIANCE STATEMENT

I certify that:

1. I have read and understood LAU's Plagiarism Policy.
2. I understand that failure to comply with this Policy can lead to academic and disciplinary actions against me.
3. This work is substantially my own, and to the extent that any part of this work is not my own I have indicated that by acknowledging its sources.

Name: Rami Issam El Raida

Signature: [redacted]

Date: 15 / 05 / 2019
Day Month Year

Acknowledgement

First and foremost, I would like to thank my family and friends for their continuous guidance and support that have helped me reach this stage. Also, this work would not have been possible without the support of Dr. Chadi AbouRjeily, my advisor in this thesis research. His experience and knowledge in the field were the foundation onto which this study was based. I would also like to thank my committee members; Dr. Dani Tannir and Dr. Wissam Fawaz, alongside all the professors in the Electrical and Computer Engineering department at the Lebanese American University who have guided me and helped me build a firm knowledge in this field. Moreover, I am grateful to all those with whom I have the pleasure to work with in the research study.

Receiver Design for MIMO FSO Communication Systems with photon-counting Detection

Rami El Mawla

Abstract

Optical wireless communication (OWC) constitutes a key technology for 5G wireless networks. OWC alleviates the radio frequency (RF) spectrum crunch problem by enabling communications in the visible, infrared and ultraviolet optical frequency bands for a variety of indoor and outdoor applications. Outdoor infrared OWC systems are widely referred to as free-space optical (FSO) communications that rely on line-of-sight transmissions of narrow laser beams. The FSO technology is license-free, easy-to-deploy, cost-effective and capable of delivering very high data rates. The major impairment that severely degrades the performance of FSO links is related to the random aspect of the atmosphere. Overcoming atmospheric turbulence-induced fading became the key research area where many solutions have been proposed and analyzed. These solutions include the multiple-input-multiple-output (MIMO) techniques.

This work investigates and compares three MIMO FSO techniques; namely, spatial-multiplexing (SMux), repetition-coding (RC) and optical-spatial-modulation (OSM). Unlike the existing literature that considers the simplistic additive white Gaussian noise (AWGN) model, this work revolves around the more accurate Poisson noise model where the number of detected photons at the receiver follows the Poisson distribution for shot-noise limited receivers. We compare the SMux, RC and OSM systems in terms of data-rate, error-rate, receiver complexity, channel estimation requirements… For each system, the optimal maximum-likelihood (ML) decoder is derived and analyzed under Poisson noise. We also evaluate the theoretical bit error rates (BERs) of RC and OSM. While the SMux and RC schemes are the most efficient in terms of maximizing the data-rate and minimizing the error-rate, respectively, the OSM scheme constitutes a practical appealing tradeoff between SMux and RC. The OSM solution leverages the need for inter-antenna synchronization while achieving improved multiplexing gains.

Keywords: Free Space Optics, Maximum Likelihood, MIMO, Repetition Coding, Spatial Modulation, Spatial Multiplexing, Gamma-Gamma, Poisson Noise, IM/DD, PPM, Equal-Gain Combining

TABLE OF CONTENTS

Chapter **Page**

List of Tables

Table of Figures

Chapter 1

Introduction & Literature Review

1.1 Free Space Optical Communication history and definition

The spread of wireless communications emerges as a standout amongst the most significant phenomena in technology. Wireless devices have turned out to be inescapable substantially more quickly than anybody could have envisioned thirty years back and they will keep on being a key component of present-day society for a long time to come [1].

The early stage of wireless communication was concentrated on the Radio-Frequency technologies which are based on electromagnetic signals for data transmission [3]. Nowadays, the term “wireless” is almost considered as a synonym of radio-frequency (RF) technologies because of the wide-scale usage of remote RF gadgets and frameworks. The RF band of the electromagnetic spectrum is however basically restricted in capacity and expensive since most sub-bands are completely licensed [1]. With the increasing use of heavy data wireless communications, the request for RF spectrum is exceeding supply and the time has come to truly consider other reasonable alternatives for remote correspondence utilizing the upper parts of the electromagnetic spectrum.

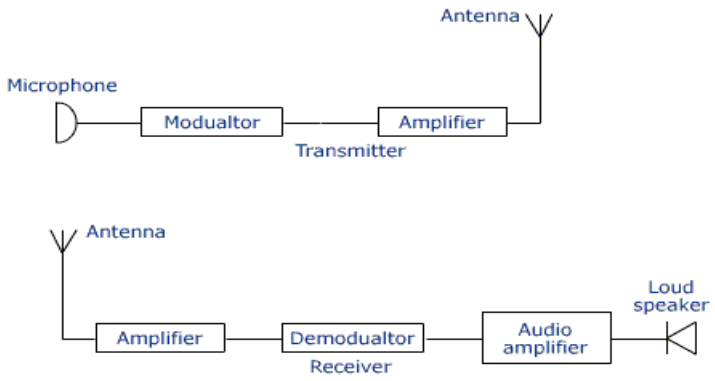

Figure 1 Block Diagram of a wireless communication system

As an alternative, researches have shifted their focus on utilizing light for data transmission instead of electromagnetic signals which is basically free space optics (FSO) for outdoor applications and visible light communication (VLC) for indoor applications. Signaling through beacon fires, smoke, ship flags and semaphore telegraph [4] can be considered the historical forms of optical wireless communication (OWC). Sunlight has been also used for long distance signaling since very early times. The original use of sunlight as a way of communication was applied during ancient Greeks and Romans who used their polished shields to send signals by reflecting sunlight during battles [2].

The early applications of this old technology was the invention of heliograph in 1810 by Carl Friedrich Gauss that was based on a pair of mirrors to direct a controlled beam of sunlight to a distant station, as well as the invention of the first wireless telephone system "photo phone" by Alexander Graham Bell in 1880 which was based on the concept one emitting vibrations through voice on a mirror at the transmitter. The vibrations were reflected and projected by sunlight and transformed back into voice at the receiver [6].

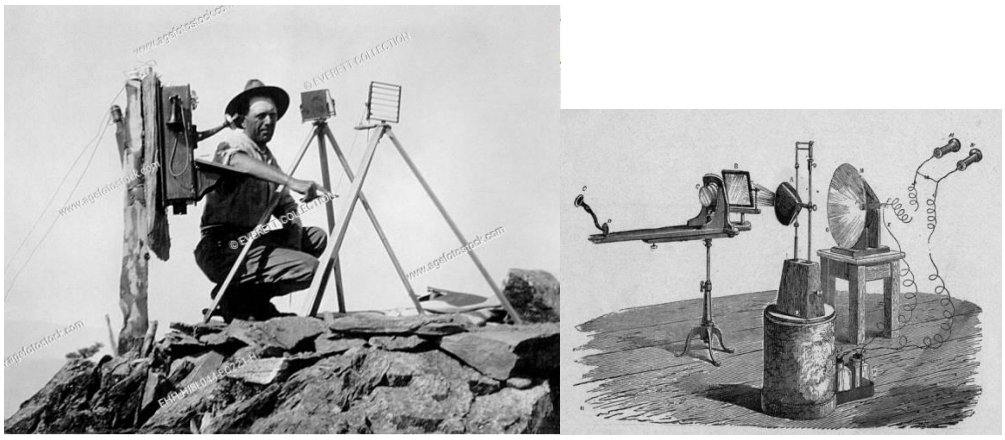

Figure 2(a) Carl Friedrich Gauss Heliograph (b) Alexander Graham Bell Photo phone

Nowadays, OWC has been evolved in a way that either lasers or light emitting diodes (LEDs) were used as transmitters. An OWC link was built using light emitting GaAs diode by MIT Lincoln Labs in 1962 that managed to transmit TV signals over a 30 miles' distance. After the invention of the laser, OWC was envisioned to be the main deployment area for lasers [7][8].

After that, the optical fiber communication has emerged due to the low loss solution that it provides over long distance communication systems. It is a technology that transmits data from source to destination via optical fiber links which are made of glass which explains the strong immunity to noise and loss [9]. However, this technology requires special installation equipment, large space and precise cabling procedure for the fragile fiberglass which increased the cost of implementing optical fiber communication [10]. Digging and installing optical fiber also constitute major factors that drastically increase the installation costs of optical fiber networks.

Moreover, this has motivated the wireless version of the optical fiber communication to arise which is the free space optical (FSO) communication.

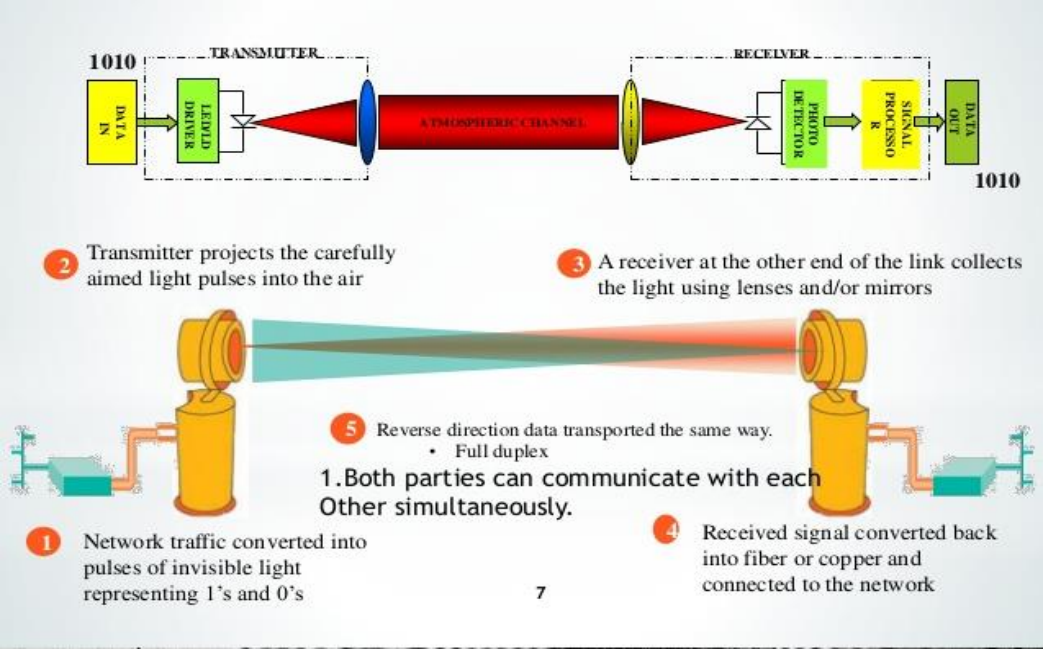

Figure 3 FSO Block Diagram

FSO communication works on line of sight technology that utilizes a laser beam by sending the very high bandwidth data from one location to another through an atmospheric channel in the absence of physical links [11]. This can be accomplished by transmitting a modulated narrow laser beams using Infrared (IR) optical carriers in the atmosphere [1]. The free space medium can be the outer space, vacuum, air or atmosphere and any equivalent medium [12].

In FSO, the transmitter contains an optical source, a modulator, an optical amplifier (if required), and beam forming optics. The data bits, which are produced by the optical source (laser or LED), are first encoded and then modulated in order to form a laser beam. The optical intensity of the modulated laser beam is then boosted through the optical amplifier. The resulted light beam is collected and refocused using beam forming optics before being transmitted through the channel [1].

It is important to mention that the commonly used optical source in FSO systems is a semiconductor laser diode (LD) [13]. High optical power is expected to be delivered from the optical source over a wide temperature range. In addition to that, it should have a long mean time between failures (MTBF) and the optical source components should be efficient as much as possible in size and power consumption [14]. Consequently, vertical-cavity-surface-emitting lasers (VCSEL) are mostly used for operation around 850 nm, [1] and Fabry-Perot (FP) and distributed feedback (DFB) lasers are mostly used for operation at 1550 nm.

At the receive side, the photodetector will detect the optical beam after being filtered, collected and refocused and then the signal will be transformed back into an electrical signal as shown in figure (3).

After noise filtration, the detected electrical signal is then demodulated to recover the initial message.

1.2 FSO Applications

Due to the huge attention that was given by the researchers and investors, FSO systems have been developed through the years to reach a position where it can be considered a trustable and promising wireless communication. For that FSO systems are being applied in many applications in small and large systems, mainly the following [15] [17].

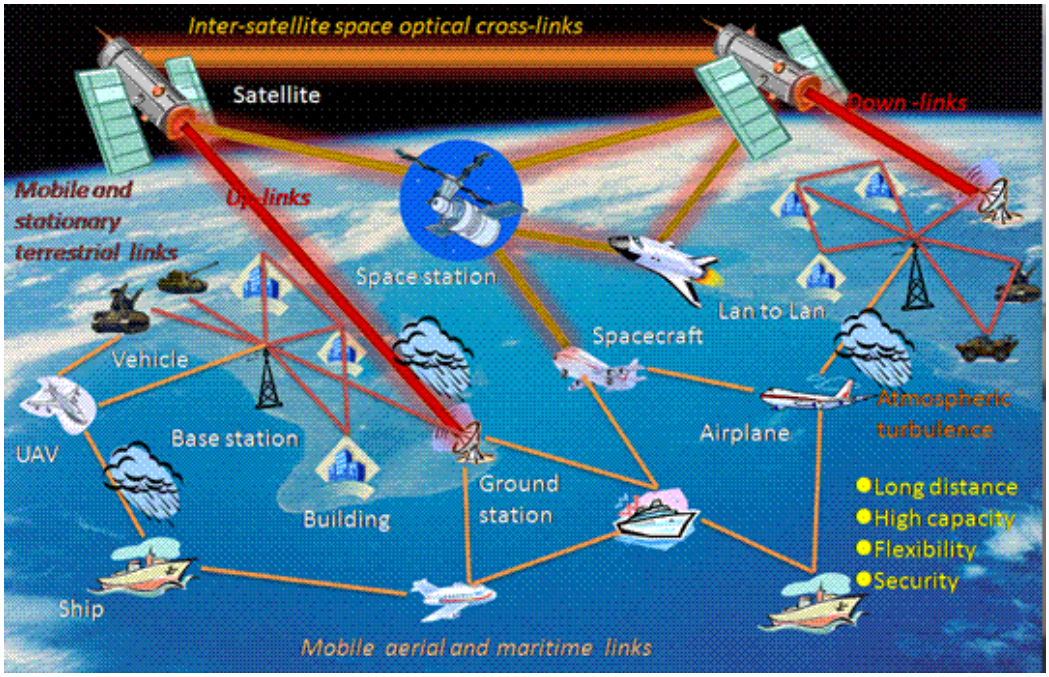

Figure 4 FSO Applications

• **Redundant link and disaster recovery**: Natural disasters, terrorist attacks, military applications, and emergency situations require flexible and inventive reactions. Temporary FSO links can be promptly installed within hours in such circumstances in which local infrastructure could be harmed or untrustworthy. A good example of this application is the 9/11 terrorist attacks in New York City where FSO links were quickly deployed in financial cooperation with no landlines to act as an efficient and redundant communication system.

• **Broadcasting**: FSO link can provide high-quality transmission between the cameras that are covering live events and the broadcasting vehicle which uses satellite uplink to connect to central. FSO links can also reach the required throughput for high definition television broadcasting applications. For example, BBC (UK) installed FSO links between local studio locations in South Africa and the central office to cover the 2010 FIFA World.

• **Enterprise/campus connectivity**: FSO systems can act as a bridge between multiple buildings in a heterogeneous network system to provide high-speed communication without the cost of fiber connections.

• **Video surveillance and monitoring**: Although wireless surveillance is easy to install, the normal wireless technologies couldn't reach the required throughput. For that, FSO links are considered as an alternative to providing required video quality and speed.

• **Back-haul for cellular systems**: The increasing number of bandwidth-intensive mobile phone services gave space for FSO to be considered as a solution to reach higher throughput.

• **Difficult terrains**: FSO links can offer a cheaper and practical solution in places where other technologies are expensive or very difficult such as crowded street, rail tracks or across a river.

1.3 FSO Advantages

• **License Free:** The narrow laser beams that are used by FSO transceivers offer a high reuse factor, intrinsic security, and sturdiness against electromagnetic interference communication. In addition to that, FSO technology does not require license fees since it operates in frequencies that are above 300 GHz which are unlicensed worldwide [18] [19].

• **High Data Rate:** FSO uses wavelength division multiplexing (WDM) which causes a higher bit rate than the promised 10 Gbps.

• **Low Cost:** FSO systems are easy to deploy and can be reinstalled without the cost of dedicated fiber optic connections [1]. For that, FSO systems are used to link multiple buildings in corporate and campus networks such as universities.

• **Low Power Consumption:** Furthermore, the FSO link requires low power since this technology uses laser and LEDs as an optical source.

• **Secured Communication:** The interception of the signal in FSO systems is much harder than the signal in RF systems due to the narrow and high directional beam of the FSO systems.

• **Easy to install:** Since there is no fiber cable installation nor any physical channel in the FSO systems and since the FSO transceiver can be easily installed even behind windows, installation of a complete FSO system can be done in days.

• **Full Duplex communication**: Since the FSO transceiver can take the role of transmitter and receiver at the same time, FSO systems are bi-directional by nature.

1.4 FSO Limitations

Due to the fact that FSO uses air as the medium of transmission, FSO faces many environmental challenges that are unavoidable. Despite all the above-mentioned advantages, we state the following limitations [31, 35]:

• **Physical Obstructions:** Due to the narrow laser beam of the optical source, small or big objects can temporarily or permanently block a single beam when it appears in the line of sight (LOS) such as birds, trees and new buildings.

• **Scintillation:** The passage of a particle (electron or high-energy photon) through a transparent material will cause a light flash or known as scintillation. In other words, the change in temperature or in atmospheric pressure will cause a change in the refractive index of the propagation path. This phenomenon will directly affect the amplitude of the FSO signal especially if the turbulent cells are comparable to the size of the optical beam which causes "image dancing" at the FSO receiver.

• **Geometric Losses:** FSO signal will lose power while traveling from the transmitter to the receiver. This loss along with the spreading of the optical beam is called geometric losses.

• **Absorption:** absorption is brought about by the water atoms which are suspended in the earthbound climate. The photons power would be consumed by these particles. The power density of the optical beam is diminished and the accessibility of the transmission in an FSO framework is specifically influenced by absorption. Carbon dioxide can likewise cause the absorption of the FSO signal.

• **Atmospheric Turbulence:** the atmospheric disturbance occurs because of the weather and environment structure mainly by wind and convection which diverse the air packets at different temperatures. This is the base of the fluctuations in the air density which eventually changes the air refractive index. The degree of the effects depends on the scale size of turbulence as per the following:

When the turbulence cell size is larger than the optical beam diameter, then the dominant effect will be beam wander which is explained as the displacement of the optical beam spot rapidly.

And when the turbulence cell size is smaller than the optical beam diameter, then the dominant effect is intensity fluctuation or scintillation of the optical beam.

• **Scattering:** is the collision of the optical beam and the scatterer. In longer distance, the intensity of the beam is reduced to the directional redistribution of optical energy. Atmospheric attenuation has the following three types.

- If the physical size of the scatterer is smaller than the size of the wavelength, then we have the Rayleigh scattering also known as molecule scattering.
- If the scatterer has comparable size to the one of the wavelength, then this the Mie scattering also known as aerosol scattering.
- And if it is bigger than the wavelength size, then a nonselective scattering occurs also known as geometric scattering.

• **Atmospheric Weather Conditions:** FSO link uses the atmosphere as the medium of transmission. The main cause of the atmospheric attenuation is the weather conditions which depends on which geographical region the FSO link is being established. Some of the weather conditions are described below.

Fog causes a severe condition which absorbs, scatters and reflects the optical beam.

Rainfall causes a wavelength independent attenuation which is the reason behind the nonselective scattering [27]. FSO system level of visibility is dependent on the size and quantity of the rain. For that, heavy rain can either modify the optical beam features or limit the passage of beam as the optical beam is absorbed, scattered, and reflected due to the size of the water droplets [29].

Haze particles can stay the air for enough time to cause an atmospheric attenuation. The stronger the haze will be, the smaller the visibility level would be and the stronger the attenuation level. There are two ways to collect

information about attenuation for checking the performance of FSO system: first, by installing system temporary at the site and check its performance and, second, by using Kim and Kruse model [27].

Smoke can be caused by carbon combustion or emission or any different substances like glycerol. Due to the thickness of its particles, it can directly affect the visibility of the transmission medium [30].

Sandstorms are a well-known limitation of outdoor link communication. The size of the wind particles, which depends on the soil textures [31], along with the speed of the wind particles are the two categories that explain the effect of sandstorms on the FSO link.

Clouds form through the condensation of the water vapor (gas particles) into visible water droplets above the earth's surface. Clouds can entirely block the optical beam from the transmitter on earth to the receiver in space. The attenuation caused by clouds is difficult to calculate because of the diversity and inhomogeneity of the cloud particles [32].

Snow contains large particles which are divided into two categories: wet and dry snow depending on the density of the particles that set the geometric scattering level. The snow particles have an impact similar to Rayleigh scattering [33].

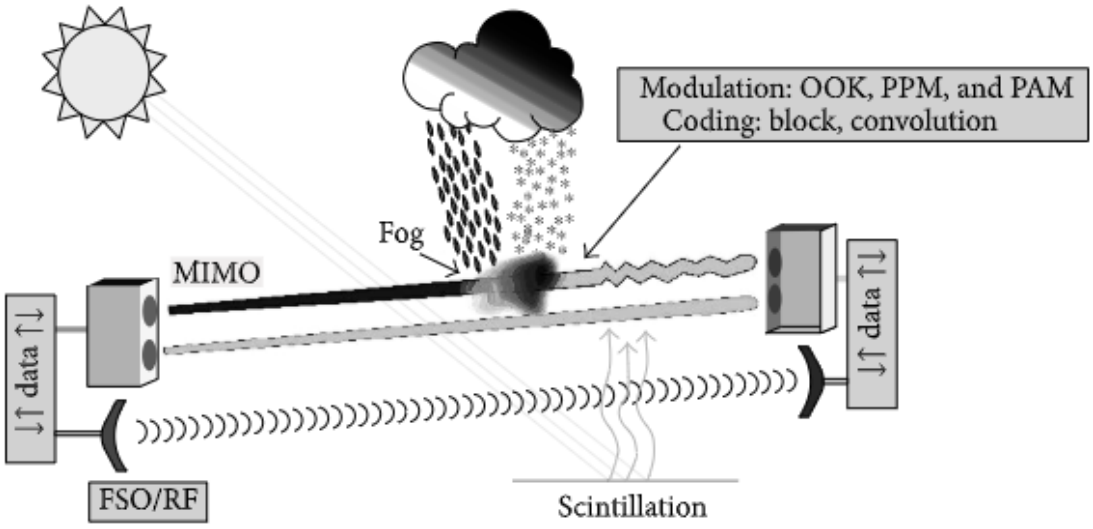

Figure 5 Atmospheric effects on FSO systems

1.5 Latest Contributions in MISO & MIMO FSO systems

Free-Space Optical (FSO) communication systems suffer from turbulence-induced fading that results in a random fluctuation of the received signal power in a way that is analogous to radio-frequency (RF) systems. Following from this impairment that severely degrades the performance of FSO links and following from all above-mentioned limitations, Multiple-Input-Multiple-Output (MIMO) techniques were advised as powerful fading mitigation strategies capable of achieving significant diversity and multiplexing gains [34]- [44].

The effect of scintillation can be reduced by using spatial diversity where there are multiple apertures at the transmitter and/or the receiver sides. The most widely studied MIMO FSO techniques revolve around repetition coding (RC), spatial multiplexing (SMux) and optical spatial modulation (OSM).

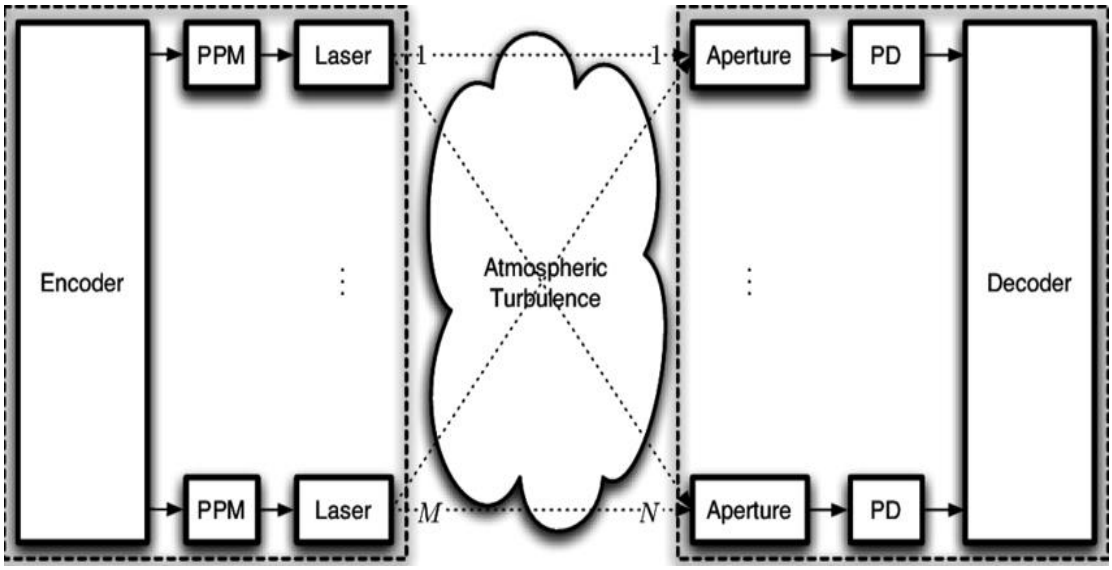

Figure 6 Block diagram of a M X N MIMO FSO system

The RC scheme is capable of achieving full diversity by simply transmitting the same information symbol from all transmit apertures. In [1], it has been demonstrated that RC outperforms orthogonal space-time codes with on-off-keying (OOK) modulation over a lognormal fading channel. The performance analysis of RC with binary pulse position modulation (PPM) was carried out in [2], [3] over gamma-gamma fading channels. On the other hand, [4] targeted the outage performance of MIMO RC systems with PPM while the ergodic capacity of MIMO RC OOK systems was evaluated in [5]. While [1]– [5] all considered the additive white Gaussian noise (AWGN) model, [6] and [7] considered photon-counting based receivers where the numbers of signal and noise photons falling at the receiver follow the Poisson distribution.

Spatial multiplexing (SMux) MIMO FSO systems were investigated in [10], [11] under the AWGN assumption. In SMux, P information symbols are transmitted simultaneously from the P transmit apertures in an attempt to maximize the multiplexing gain.

The performance of MIMO FSO systems over fading channels has been widely examined in terms of outage probability and error rate, however, few studies were concentrated on the theoretical ergodic capacity due to the mathematical

difficulty of solving the integral of the ergodic capacity. Lately, the ergodic capacity of MIMO FSO communications using multiple partially coherent beams propagation through strong turbulence channels has been studied in [57] by using a single approximation. However, the approximation results presented in [57] need an adjustment parameter to obtain a sufficient approximation accuracy. In [43], a more accurate approximation method was used to assess the capacity of MIMO FSO systems by approximating the probability density function (pdf) of the SNR at the receiver by using the $\alpha - \mu$ distribution of which the authors have provided the cumbersome statistical ergodic capacity analysis of MIMO FSO systems with EGC over turbulence channels, which are modeled as independent and identically distributed (i.i.d.) and independent, but not necessarily identically distributed (i.n.i.d.) distributions, respectively.

For this multiple-input-multiple-output (MIMO) systems, combining the information bearing symbols at the transmitter in order to optimize the system performance is classically called space-time (ST) coding.

In classical MIMO FSO systems, ST coding is not needed at the transmitter and the same symbol is sent over the multiple beams. This is usually referred to as repetition coding (RC) [44]. On the other hand, most of the orthogonal ST block codes (OSTBCs) can be modified to be adapted to IM/DD FSO systems. For instance, for the case of two transmitter beams, a modified Alamouti scheme [58] is proposed in [59] which is adapted to IM/DD optical systems by introducing a bias to overcome unipolar signaling used in these systems. This idea is then generalized in [60] to ON-OFF keying (OOK) modulation with any pulse shape. In fact, Both RC and OSTBCs provide full diversity but RC is shown to outperform the latter, and the performance gap increases with an increased number of transmitter beams [40]. In fact, RC seems to be quasi-optimum, as explained in [62]. Still, it doesn't exploit the MIMO channel to increase the transmission rate. In opposite, SMux maximizes the transmission rate but at the cost of reduced diversity gain. Recently, a new signaling scheme called optical spatial modulation (OSM) has been proposed by which only one ON symbol is transmitted from one out of the P beams at a given channel use

[61], [63] so as to avoid inter-channel interference. The data rate of OSM is $log_2(P)$ bits per channel-use. At the receiver, optimal maximum likelihood detection (MLD) can be used to estimate the index of the corresponding activated beam [64].

The authors of [65] studied the problem of feedback based beamforming for multiple-input single-output free (MISO) FSO system with pointing errors. For a 2×1 FSO system, it was shown theoretically that any arbitrary beamforming scheme performs poorer to the repetition coding scheme but achieves full diversity over the Gamma-Gamma fading with pointing errors. Also, the authors of [65] have studied a beamforming scheme for 2 × 1 FSO system which employs one-bit feedback from the receiver to the transmitter. Erroneous feedback leads to a loss in diversity for this beamforming scheme as established by the bit error rate (BER) analysis. For avoiding the loss in diversity, an improved one-bit feedback based beamforming scheme was proposed which outperforms the repetition coding.

In [66], an arbitrary beamforming scheme is analyzed in a 2 × 2 multiple-input-multiple-output (MIMO) FSO communication system. The probability density function (PDF) and moment generating function (MGF) of the instantaneously received signal-to-noise ratio (SNR) in the receiver are derived for Gamma-Gamma distributed non-identical FSO links. The authors of [66] also considered the effect of zero-boresight misalignment errors where the radial misalignment is assumed to be Rayleigh distributed. Using the MGF of the SNR, the error performance of the considered FSO system is investigated. Specifically, authors of [66] derived the expression for the average symbol error rate (SER) for subcarrier intensity modulated (SIM) M-ary phase shift keying (MPSK). Contrary to the fact that repetition scheme (equal weight beamforming) is optimal in identical channel conditions, it is observed in [66] that for non-identical turbulence channels, arbitrary beamforming with proper selection of weights can outperform the repetition beamforming.

1.6 Different types of channels

In this section, we highlight on the different channel models adopted in the open literature for characterizing the scintillation conditions along atmospheric turbulence FSO links.

1.6.1 Lognormal Channel

The lognormal distribution is widely used to model medium-scale fading along RF wireless channels. This same distribution can be used to model FSO channels with weak-to-average scintillation. In this section, we highlight on the different channel models adopted in the open literature for characterizing the scintillation conditions along atmospheric turbulence FSO links.

When evaluating the performance of MIMO FSO systems, the computation of the outage probability consists of getting the mean and variance of the sum of lognormal random variables. There is still no general closed-form expression for the lognormal sum distribution but only several approximation methods with highly nonlinear function.

The probability density function (pdf) of the lognormal distribution is

$$f(x|\mu,\sigma) = \frac{1}{x\sigma\sqrt{2\pi}}\, exp\left\{\frac{-(\ln x-\mu)^2}{2\sigma^2}\right\} \; ; x > 0 \qquad (1.1)$$

Where μ and σ are respectively the mean and the standard deviation of the logarithmic values

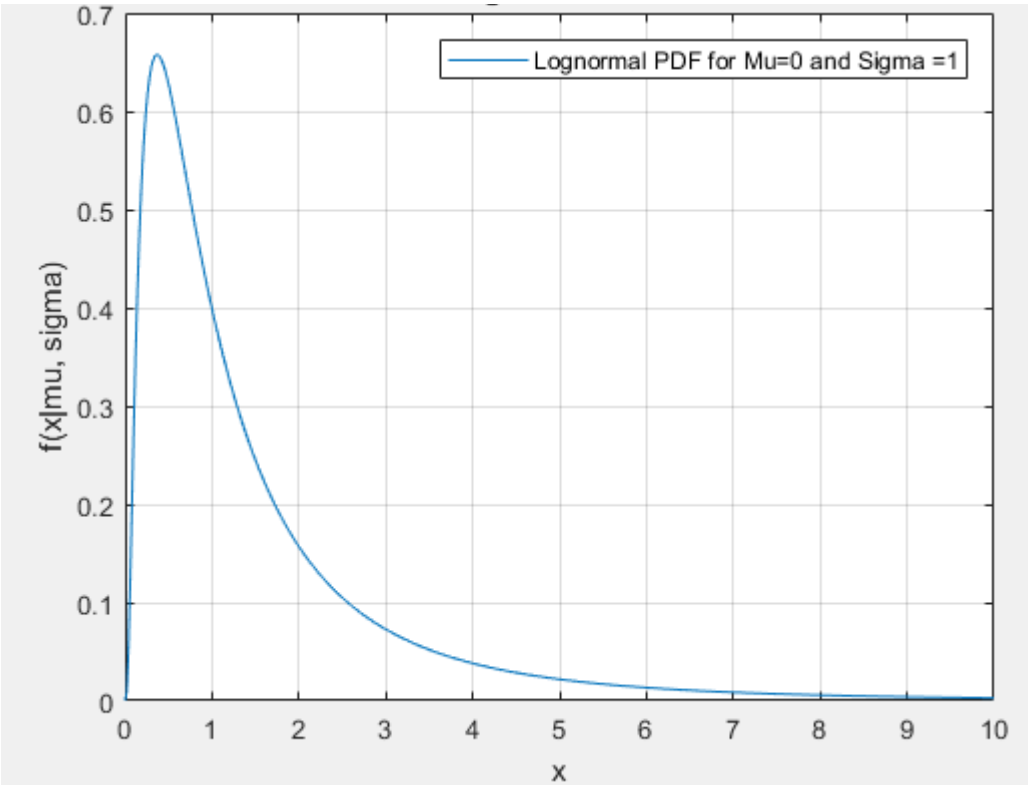

Figure 7 PDF of the lognormal distribution

1.6.2 Rayleigh Channel

Rayleigh fading can be a useful model when there are many scatterers between the transmitter and the receiver that diffuse the light signal such as heavily built-up city centers. In a large amount of scattering, then the channel impulse response will be modeled as Gaussian, despite the distribution of individual components of the signal. In the absence of the dominant component, there will be a fully distributed phase between 0 and 2π radians, thus having zero mean. The envelope thus formed will be Rayleigh distributed.

The probability density function (pdf) of the Rayleigh distribution is

$$y = f(x|b) = \frac{x}{b^2} e^{\left(\frac{-x^2}{2b^2}\right)} \tag{1.2}$$

Where b is the scale parameter of the Rayleigh distribution

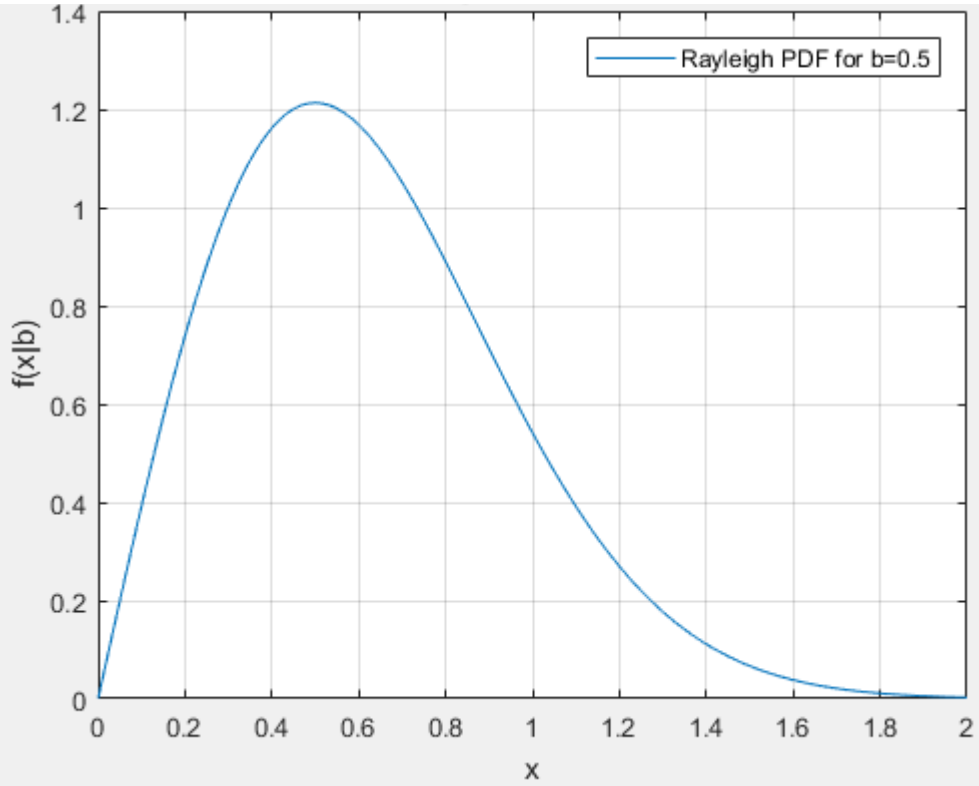

Figure 8 PDF of the Rayleigh distribution

1.6.3 Gamma-Gamma Channel

The Gamma-gamma distribution can be used with a very broad range of turbulence.

In this work, we adopt the widely approved gamma-gamma channel model where the probability density function of I_P , the channel irradiance between the p-th transmit aperture and the receive aperture, is given by:

$$f(I) = \frac{2(\alpha\beta)^{(\alpha+\beta)/2}}{\Gamma(\alpha)\Gamma(\beta)} I^{(\alpha+\beta)/2-1} K_{\alpha-\beta}\left(2\sqrt{\alpha\beta I}\right) \quad (1.3)$$

where $\Gamma(.)$ is the Gamma function and $K_c(.)$ is the modified Bessel function of the second kind of order c. The parameters are:

$$\alpha = \left[exp\left(0.49{\sigma^2}_R/\left(1 + 1.11{\sigma^{12/5}}_R\right)^{7/6}\right) - 1\right]^{-1} \quad (1.4)$$

$$\beta = \left[exp\left(0.51{\sigma^2}_R/\left(1 + 0.69\,{\sigma^{12/5}}_R\right)^{5/6}\right) - 1\right]^{-1} \quad (1.5)$$

Which depend on the link distance$d$ through the Rytov variance

$${\sigma^2}_R(d) = 1.23\, C_n^2 \left(\frac{2\pi}{\lambda}\right)^{7/6} d^{11/6} \quad (1.6)$$

Where C_n^2 denotes the refractive index structure parameter, λ is the wavelength of light and d is the link distance between the transmitter and receiver.

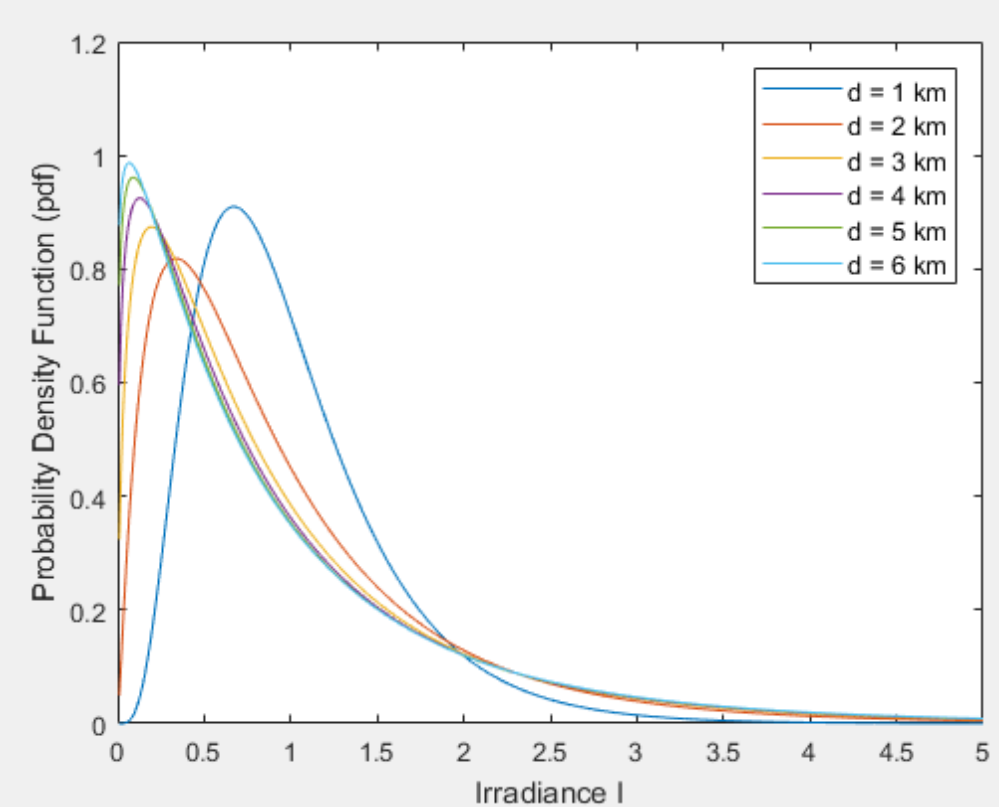

Figure 9 PDF of Gamma - Gamma distribution for different distances

1.7 Different types of modulation

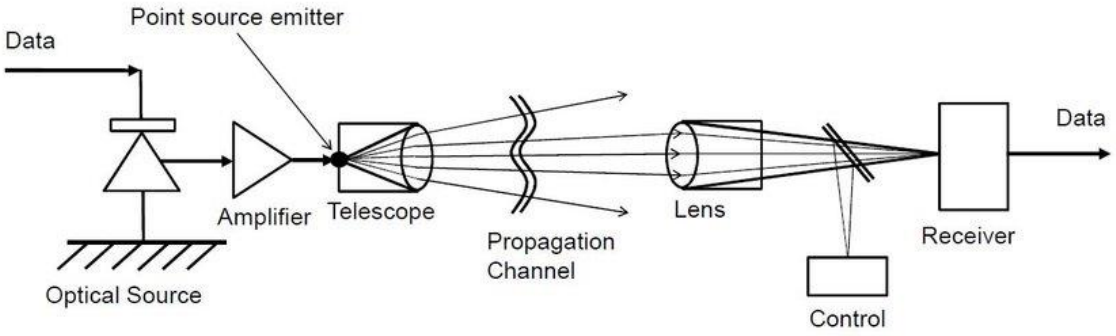

Figure 10 Block diagram of an IM/DD FSO channel

The optical transmission system consists of optical signal modulation, transmission, detection, and demodulation. In FSO systems, optical source signal intensity is modulated before being transmitted through the channel. This modulation can take place in the following: amplitude, frequency, phase, and polarization. FSO systems can use different types of modulation that can be comparable in terms of the average received optical power required to reach desired BER at the given data rate. A power-efficient modulation scheme is desirable in order to minimize the ratio of peak to average power. The most usable modulation scheme in free space optics is the intensity modulation direct detection (IM/DD) scheme [53].

1.7.1 Intensity Modulation / Direct Detection (IM/DD)

It is the process of modulating the laser source directly by the analog modulating signal. The intensity of the optical signal is varied in accordance with the amplitude of the modulating signal. The receiver consists of a photodetector to convert the optical signal to electrical form and then passed through a low-pass filter to get the modulating signal.

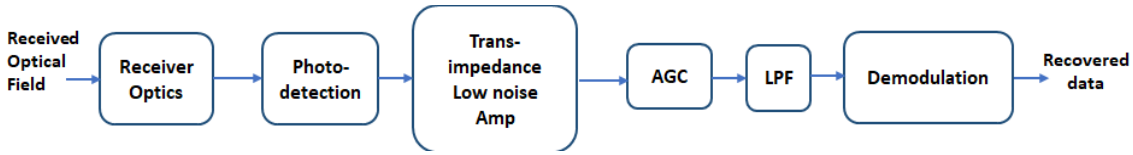

Figure 11 IM-DD FSO receiver block diagram

The type of modulation scheme should be chosen based upon power efficiency, bandwidth efficiency, simple design requirement, low-cost implementation and immunity to interference and background radiations. [4]

1.7.2 On-Off Keying Modulation

As one of the many IM schemes, OOK is easily implemented with an appealing bandwidth efficiency. This modulation scheme needs an adaptive threshold in turbulent atmospheric conditions for best results [54]. Based on that, the light source will be used a logical signal either “One” for on status or “Zero” for off status. OOK is affected by amplitude distortion i.e. fading and propagation of the signal. Coherent modulation schemes such as binary phase shift keying (BPSK) and differential phase shift keying (DPSK) can also be used at the expense of an increased complexity.

The advantage of coherent modulation technique is that the error probability decreases but the system becomes more complex.

The receiver structure consists of the following:

- A filter, sampler and threshold device
- Tested esteem compared against the predetermined threshold and bit is detected
- Requires replica carrier at the receiver.
- Received signal and replica carrier are cross-correlated using the information contained in their amplitude and phase

Based on the above reasons, subcarrier BPSK has a better BER performance than that of OOK but a more complexed one. For that, OOK systems took preference in optical links through the atmosphere.

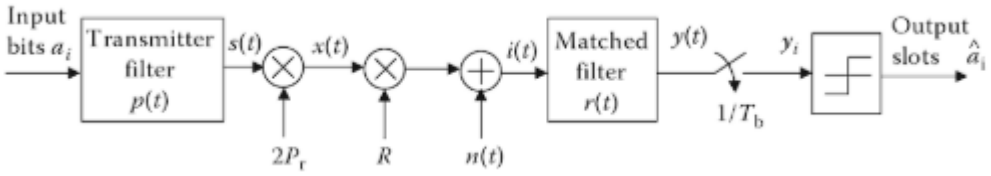

Figure 12 Block Diagram of OOK system

In non-coherent digital modulation technique, there is no use of the two carriers (at transmitter and receiver) to be phase locked. Although in non-coherent technique, the system becomes simple the error probability increases which is in contrast to the coherent detection method.

1.7.3 Pulse Position Modulation (PPM)

An interesting alternative to OOK is PPM.

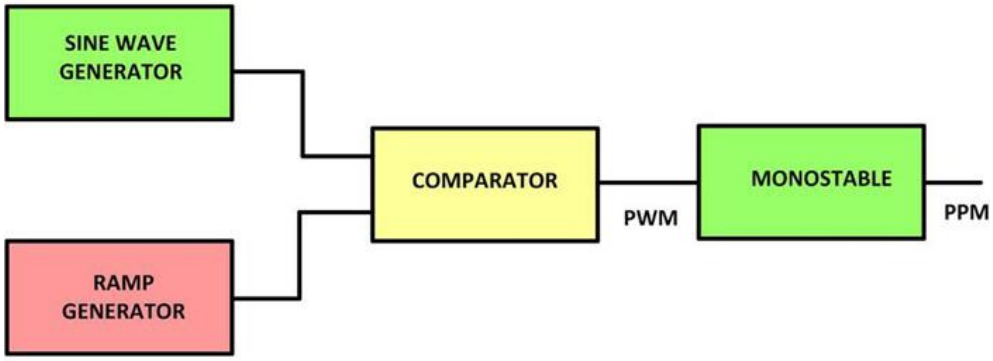

Figure 13 Block diagram of Pulse Position Modulation (PPM)

For the Q-are PPM modulation, a symbol corresponds to $\log_2 Q$ bits. The symbol duration T_s is divided into Q time slots (or chips) of duration $T = T_s/Q$ and an optical pulse is sent in only one of the Q available slots. Since Q-ary PPM

contains one pulse per Q slots, it has a duty cycle of 1/Q and a peak-to-average power ratio (PAPR) of Q. We can vary Q to make a flexible compromise between power efficiency and bandwidth efficiency. For notational simplicity, we denote the Q-ary PPM by QPPM and we will denote the binary PPM by BPPM. The important advantage of PPM over OOK is that it is more average energy efficient. In fact, to achieve a given BER, the required average power by OOK is more than that of QPPM for $Q > 2$. But at the same time, it has some disadvantages. For the same data transmission rate, more bandwidth is in general required than for OOK. The bandwidth requirement is not considered a limitation due to the huge bandwidth that FSO systems provides. However, the real challenge with a larger Q is the augmented required switching speed for electronic circuits. Moreover, the receiver synchronization becomes more difficult [56]. Another disadvantage of PPM is that for given average transmission power, by increasing Q, the PAPR increases.

1.7.4 Pulse Amplitude Modulation (PAM)

For this type of modulation, the information is encoded by varying the amplitude of the carrier pulses. There are two types of PAM, single polarity where DC bias is added to assure that all pulses are positive and double polarity where pulses can be negative and positive. FSO communications use single polarity PAM due to the non-negativity of the optical links. Depending on the number of values that a symbol can take, we can classify PAM whether binary or M-ary.

PAM is classified as one of the low complexity and bandwidth efficient modulation. It allows efficient and quick transfer of data while increasing data throughput by the mean of a simple and non-complex circuit. [55]

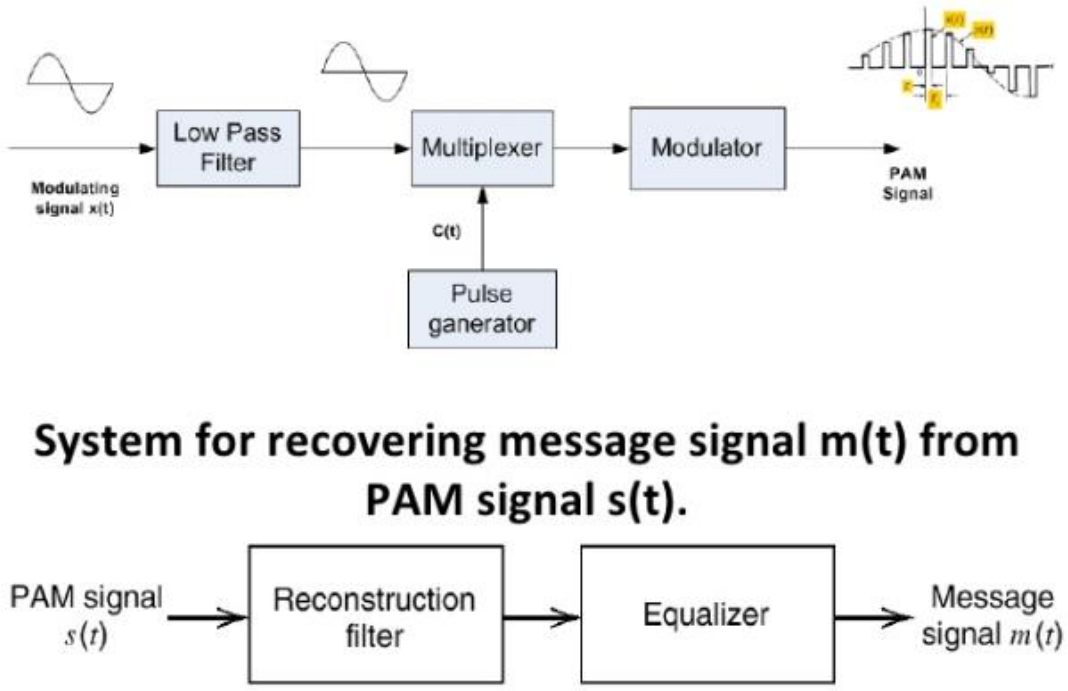

Figure 14 Block diagram of PAM generation

The following steps can describe the above block diagram:

- The role of low pass filter is to transform the train of weighted impulse functions to a train of pulses with the required shape
- The uniform sampling takes place in the multiplexer
- The purpose of the modulator is to convert discrete amplitude serial symbols into an analog output.
- Due to the amplitude distortion caused by the reconstruction filter and due to the phase delay distortion, an equalizer is needed to recover the signal.

1.8 Different types of noise models

1.8.1 Additive white Gaussian noise (AWGN)

Additive white Gaussian noise (AWGN) is an elementary noise model to imitate the consequence of many random natural processes. It has the following characteristics:

- Additive because the noise is added to the information-carrying signal. The noise is independent of the signal.
- White refers to the uniform power distribution across the frequency band of the information system.
- Gaussian because it follows a normal distribution in the time domain with an average time domain value of zero.

The summation of many random processes will lean towards having a Gaussian (or normal) distribution. The term AWGN is frequently used as a channel model in which the only impairment to communication is a linear addition of wideband or white noise with a constant spectral density (expressed as watts per Hertz of bandwidth) and a Gaussian distribution of amplitude. The model does not account for fading, frequency selectivity, interference, nonlinearity or dispersion.

However, it produces simple and tractable mathematical models which are useful for gaining insight into the underlying behavior of a system before these other phenomena are considered.

The AWGN channel model is a good model for many satellite and deep space communication links. It is not a good model for terrestrial links because of multipath, terrain blocking, interference, etc. However, for terrestrial path modeling, AWGN is commonly used to simulate background noise of the channel under study, in addition to multipath, terrain blocking, interference, ground clutter, and self-interference that modern radio systems encounter in terrestrial operation.

1.8.2 Poisson Noise

Shot noise or Poisson noise is a type of electronic noise which can be modeled by a Poisson process. In electronics, shot noise originates from the discrete nature of the electric charge. Shot noise also occurs in photon counting in optical devices, where shot noise is associated with the quantized nature of light.
The shot noise in an optical wireless channel results from the high rate physical photo electronic conversion process, with variance at the i-th PD

$$\sigma_{shi}^2 = 2qB(\gamma h_i x_j + I_{bg} I_2) \tag{1.8.2.1}$$

In day-time outdoor communications, shot noise is the dominant noise component

$$N_{shot} = 2qB \tag{1.8.2.2}$$

where q is the electronic charge, γ is the detector responsivity, B is the corresponding bandwidth, I_{bg} is background current, and I_2 is the noise bandwidth factor. Furthermore, the thermal noise is generated within the transimpedance receiver circuitry and its variance is given by

$$\sigma_{thi}^2 = \frac{8\pi K T_k}{G} \eta A I_2 B^2 + \frac{16\pi^2 K T_k \Gamma}{g_m} \eta^2 A^2 I_3 B^3 \tag{1.8.2.3}$$

where K is Boltzmann's constant, T_k is the absolute temperature, G is the open-loop voltage gain, A is the PD area, η is the fixed capacitance of the PD per unit area, Γ is the field-effect transistor (FET) channel noise factor, g_m is the FET transconductance, and
I_3= 0.0868.

For large average numbers of generated photons, the Poisson distribution approaches a normal distribution about its mean, and the elementary events (photons, electrons, etc.) are no longer individually observed, typically making shot noise in actual observations indistinguishable from the thermal Gaussian noise.

An event occurs 0, 1, 2… times in an interval. The average number of events in an interval is designated by lambda λ. Lambda is the rate parameter.

The Poisson probability density function is the following:

$$f(x\,|\lambda) = \frac{\lambda^x}{x!}e^{-x} \qquad x = 0, 1, 2, \ldots, \infty \tag{1.7}$$

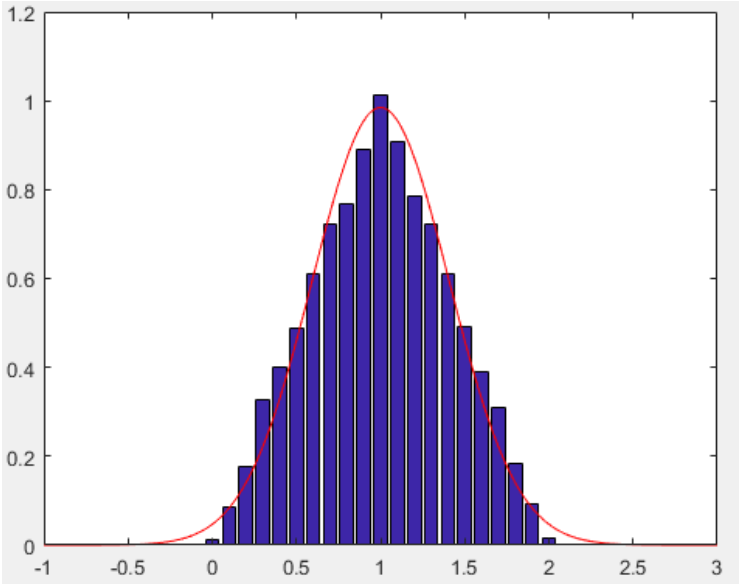

Figure 15 Probability density function of Poisson Distribution

1.9 RC, OSM and SMux schemes overview

The previously delineated RC, OSM and SMux schemes will be further detailed in this section.

1.9.1 RC Scheme:

For the RC scheme, the same information symbol is transmitted from all apertures and this solution can be implemented in the absence of channel state information (CSI) and feedback since non-coherent detection can be applied at the receiver which makes RC an appealing scheme in FSO communication systems.

Moreover, the transmit power is equally split among the transmit apertures. Due to the non-negativity of the irradiances, the RC scheme is better adapted to FSO systems with IM/DD which ensures non-destructive interference at the receiver side.

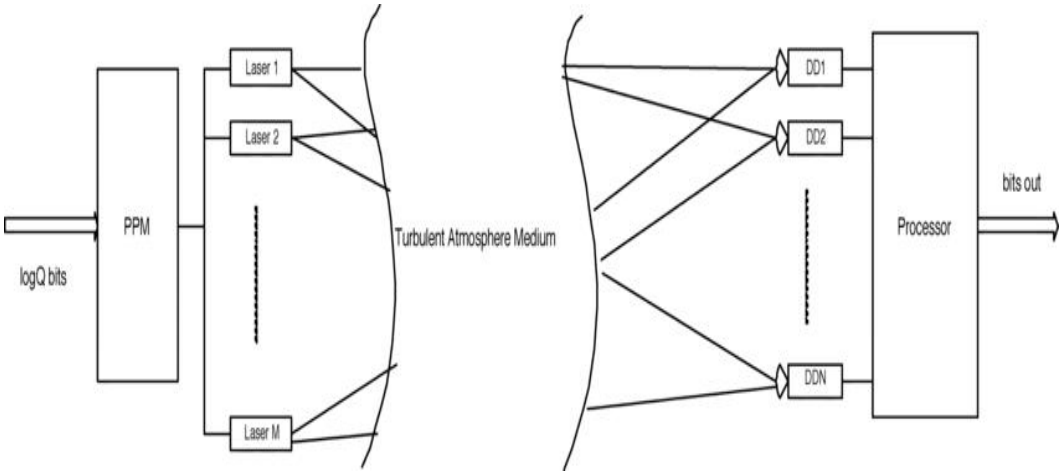

Figure 16 RC Scheme in MIMO system

1.9.2 OSM Scheme:

In order to mitigate the interference between the different transmit apertures, the OSM scheme is defined as pulsing one transmit aperture per symbol duration [46], [47]. The pulsed aperture will transmit a light signal in one PPM slot.

In spatial modulation (SM), as per figure (17), the input bits 011 is carried concurrently over both the signal and antenna spaces. The incoming data bits are divided into two parts: A first part that determines the index of the transmit aperture to be pulsed and a second part that indicates the PPM slot in which a light signal is transmitted.

As part of the SM literature, this scheme offers better multiplexing gains and error performances than conventional methods. Furthermore, since only one antenna is active in each signaling period, the transmit chain is simplified and the inter-channel-interference (ICI) is completely avoided. Note that space shift keying (SSK) has also emerged as a special form of SM where no modulation is used and only the antenna space is utilized to convey information (with no PPM modulation).

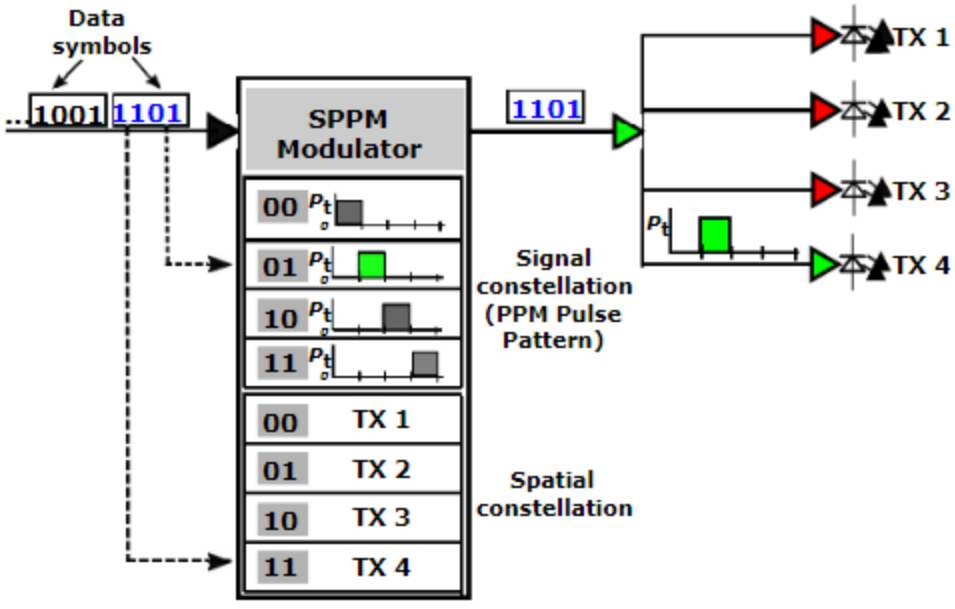

Figure 17 Illustration of Spatial Modulation scheme

1.9.3 SMux Scheme:

SMux scheme consists of transmitting independent data streams from the P transmit apertures [48], [49] which will cause a P-fold increase in the data rate. The cardinality of the transmitted constellation (that is equal to M^P) increases exponentially with the number of transmitting apertures thus complicating the detection procedure.

As per figure (18), each transmitter directs independent information to the center of its related receiver aperture. To minimize the cross-talk between channels due to the pointing error and beam divergence at the receiver, the receiver apertures must be sufficiently separated.

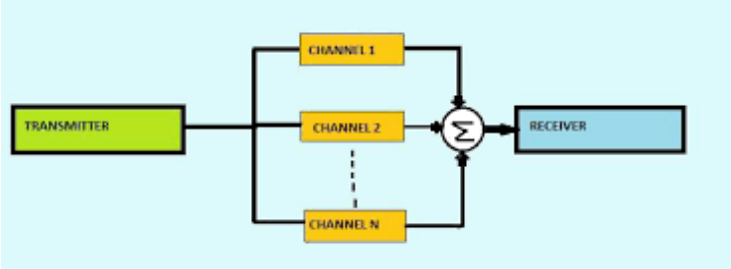

Figure 18 SMux Scheme

1.10 Maximum Likelihood (ML) Decoder

It is a symbol-by-symbol maximum-likelihood (ML) detector where it uses the channel's statistics for determining the threshold in the detection process of the bits.

This receiver decision is based on the number of photons detected in each of the M PPM slots.

Taking into consideration that there are Q receivers and that each symbol is divided into M slots., the ML decoder procedure is based on the following decision variables:

$R_{q,m}$(for $q = 1, \dots, Q \; and \; m = 1, \dots, M$)

The ML decoder operates by finding the maximum of the following probability:

$$\hat{m} = arg\ max_{\,m \in \{1,..M\}^p} \prod_{q=1}^{Q} \prod_{m=1}^{M} \Pr\left(R_{\,q,m} = r_{q,m} \middle| m\right) \tag{1.10}$$

Where:

$R_{q,m}$: random variable of the number of photons in slot m at receiver q.

$r_{q,m}$: actual number of photons detected in the m-th PPM slot m at q-th receiver aperture.

m: is the slot where the optical signal has been transmitted.

The main challenge behind this decoder under Poisson statistics exist in the fact that the weighing coefficients depend mutually on the transmitted symbols and the channel coefficients which increases the complexity of the decoder that is represented by the number of multiplications required to evaluate the weighing coefficients.

This added complexity will be linked to an improved near-optimal performance levels as will be shown later in our results.

1.11 Equal Gain Combining (EGC) Decoder

Instead of basing its decision on the QM random variables $R_{q,m}$(for $q = 1, \dots, Q \; and \; m = 1, \dots, M$), the EGC decoder bases its decision on the summation of the numbers of photoelectrons detected by the different receiver apertures in each of the M PPM slots.

The EGC decoder operates by finding the maximum of the following probability:

$$max_{m-1,\dots,M} \Pr\left(r_{1,m} + r_{2,m} + \cdots + r_{Q,M}\right) \tag{1.10}$$

Where:

$r_{q,m}$: actual number of photons detected in the m-th PPM slot m at q-th receiver aperture.

The main advantage of the EGC decoder is the lower complexity that accompanies it since only additions operations are required to find the optimal decision and no multiplications are required since the decision is not based on the weighing coefficients.

However, this will decrease the performance of the receiver as proved later.

1.12 Aim of this work

(i) To compare RC, OSM and SMux schemes for MIMO IM/DD FSO systems with both ML and EGC receivers.

(ii) To derive the symbol error rate of the RC and OSM schemes theoretically, we also show that the mathematical derivation match the numerical results obtained by Monte Carlo simulations. To confirm numerically that the OSM scheme can be seen as a tradeoff between the RC and SMux schemes improving the rate compared to RC while loosening up some usage limitations with respect to SMux.

1.13 Contributions

The aims mentioned in section 1.12 rely on the following contributions:

(i) In the literature [46] – [48], OSM and SMux were analyzed solely in the context of AWGN noise. In this work, we extend the previous results to the Poisson noise model that significantly modifies the structure of the maximum-likelihood (ML) receiver.

(ii) References [38] – [49] focus on each scheme separately, this paper compares all three schemes together and for MIMO systems. Previous studies compared the same for MISO systems and others compared all three schemes for AWGN noise.

(iii) In this work, we develop the ML and EGC decoders and we evaluate their complexities in a comprehensive manner.

(iv) Unlike usual studies that use numerical methods in evaluating the symbol error rate, the additional contribution of this work is that we derive and test the theoretical methods for the error rate analysis of the RC and OSM schemes.

(v) This work extends the previous results of the SMux results to consider the case of three transmit apertures.

Chapter 2

System Model and Transmitter structure

1.14 2.1 Channel modeling: gamma-gamma fading

For a wide range of turbulence conditions (weak to strong), the channel irradiance in FSO systems can be modeled by a Gamma-Gamma distribution as stated previously where parameters $\alpha > 0$ and $\beta > 0$ are linked to the so-called scintillation index S.I. $\triangleq 1/\alpha + 1/\beta + 1/(\alpha\beta)$. The parameters α and β can be adjusted to achieve a good agreement between the channel model and the measurement data [8], [9]. We note that PDF in (1.3) contains the K–distribution ($\alpha > 0$ and $\beta = 1$) and the negative exponential (NE) distribution ($\alpha \to \infty$ and $\beta = 1$) as special cases. The K–distribution is typically used to model strong turbulence conditions [9], [10], [12], [17], while the NE distribution can be seen as a limit distribution for extremely strong turbulence [8] and has been used in the literature mostly because of its mathematical tractability [7], [28].

1.15 2.2 Transmitter apertures and optical power

FSO communication systems can be associated with either LED transmitters or laser transmitters.

2.2.1 LED optical transmitter:

A LED is a semiconductor p–n junction device that emits incoherent light over a wide spectrum.

The transformation from electric power to optical power has a fair efficiency which results in small heat emission compared to incandescent lights.

It is mainly used for short-range FSO systems (shorter than 1 km) such us UV communication and indoor FSO systems with an output light range of 30-60 nm.

LED has the following types where LEDs with directional emitting patters are preferred for FSO communications:

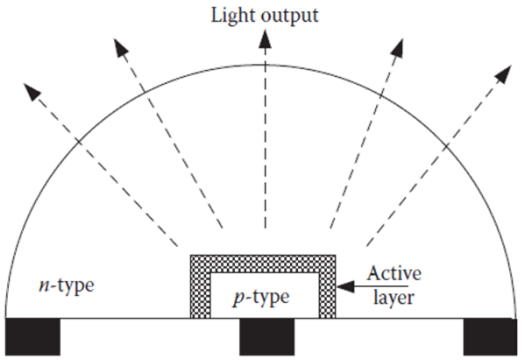

Figure 19 Dome LED

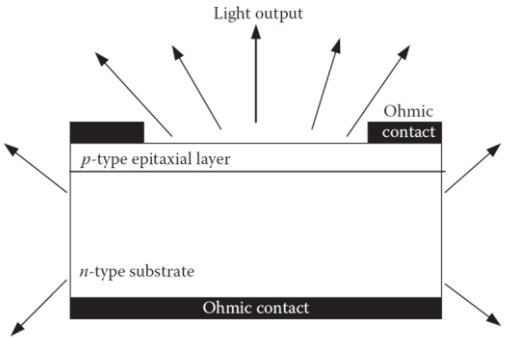

Figure 20 Planar LED

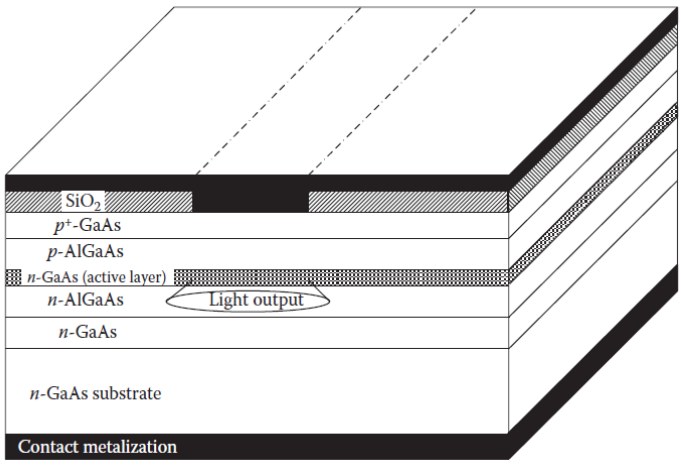

Figure 21 Edge - Emitting LED

2.2.2 Laser Optical Transmitter

Laser diodes can emit a high output power in the order of 100 mW. The light is amplified by stimulated emitted radiation and this generates coherent light. This means that light is nominally emitted on a single frequency which decreases the modal dispersion.

Laser diodes output is more directional than of a LED and can be directly modulated with high data rates.

With all of the above advantages, some drawbacks of Laser diodes are the high cost and their sensitivity to temperature which requires feedback control systems to operate properly.

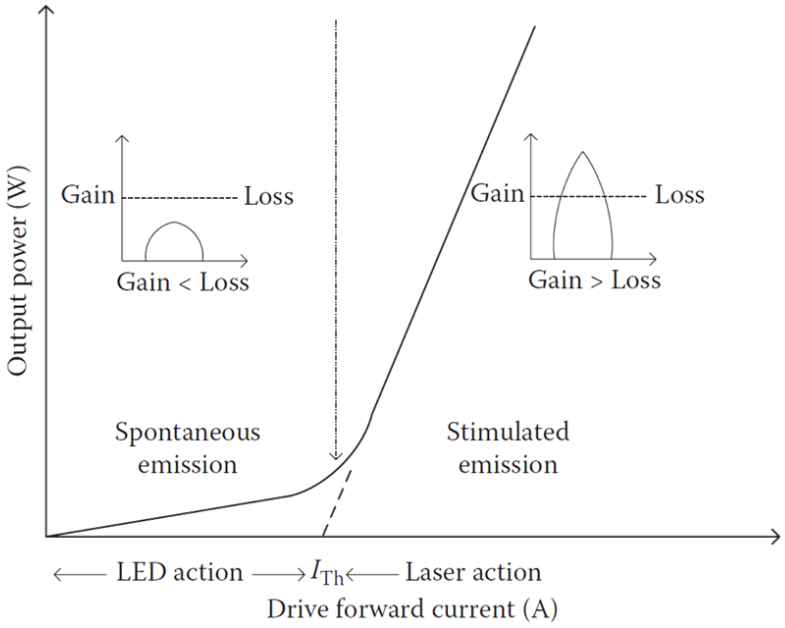

Figure 22 Laser output power against drive current plot

1.16 2.3 System Model

Consider a $P\ x\ Q$ MIMO FSO System with P transmit apertures and Q receiver apertures. Using M-ary pulse position modulation, each symbol duration T_s is divided into M slots.

Denote by P_s the optical power of the signal falling on the receiver and by P_b the optical power of background noise and the dark currents.

With no scintillation, the number of photons in an "on" (resp. "off") slot will follow the Poisson distribution with parameters $\lambda_s + \lambda_b$ (resp. λ_b) where the quantities λ_s and λ_b are given by:

$$\lambda_s = n\ \frac{P_s T_s/M}{hc/\lambda} \tag{2.3.1}$$

$$\lambda_b = n\ \frac{P_b T_s/M}{hc/\lambda} \tag{2.3.2}$$

Where n is the detector's quantum efficiency.

h is Planck's constant, c is the speed of light and λ is the wavelength.

$E_s = P_s T_s/M$ is the received optical energy per PPM slot.

The average number of photoelectrons generated by the information-carrying light signal (in the absence of scintillation) in a PPM slot will be denoted by λ_s. Similarly, the average number of noise photoelectrons generated by background radiation (and dark currents) in a PPM slot will be denoted by λ_b.

Moreover, denote by $I_{p,q}$ the channel irradiance from the p-th transmit aperture to the q-th receiver aperture.

We adopt the commonly approved gamma-gamma channel model where the probability density function of $I_{p,q}$ is given as per equations (1.3) to (1.6).

We assume that the channel irradiances $I_{p,q}$ are independent and identically distributed assuming the large separation between the elements of the transmitter and receiver arrays.

In the developed mathematical analysis presented later, we consider the case of MISO systems where the receiver is equipped with a single aperture. This simplifies the ML receiver structure and all the subsequent theoretical evaluation. For this scenario, the index q can be dropped and the irradiance between the p-th transmit aperture and the receiver aperture will be denoted by I_p for simplicity.

We denote by R_m the random variable corresponding to the number of photons detected at the receiver in the m-th PPM slot for $m = 1, \dots, M$.
R_m will follow the Poisson distribution with the following parameter:

$$E[R_m] = \frac{\sum_{p \epsilon A} I_p}{P} \lambda_s + \lambda_b \tag{2.3.3}$$

Where $E[.]$ stands for the averaging operator while the division by P results from evenly splitting the transmit power among the P transmit apertures to have the same power as in single-aperture systems. The parameters λ_s and λ_b are given in (2.3.1) and (2.3.2), respectively. In (2.3.3), A stands for the set of transmit apertures that are pulsed in the corresponding PPM slot. If none of the apertures is pulsed in a given PPM slot, then the photons will be generated exclusively by background radiation.

Chapter 3

Comparing the Transmission Schemes with Optimal Detection

3.1 Repetition Coding (RC)

3.1.1 Derivation for ML and EGC decoders for MISO and MIMO systems

Under the assumption that the PPM symbols m∈{1,…,M} has been transmitted, and following from sections 1.9.1 and 2.3, the parameters of the M decision variables are given by:

$$\mathrm{E}\,[R_{q,m'}] = \begin{cases} \frac{\lambda_s}{P} \sum_{p=1}^{P} I_{p,q} + \lambda_b & m' = m \\ \lambda_b & m' \neq m \end{cases} \tag{3.1}$$

where all lasers are transmitting concurrently in the m-th slot while all remaining slots are empty (and, hence, comprise only the contribution of noise/background radiation).

The ML decoder decides in favor of symbol $\hat{m}$ as per below equation

$$\hat{m} = \arg max_{m=1,\dots,M} \Pr(R = r \mid m) \tag{3.2}$$

Where $R = [R_{1,1} \dots R_{1,M} \dots \dots R_{Q,1} \dots R_{Q,Q}]$, $[r_{1,1} \dots r_{1,M} \dots \dots r_{Q,1} \dots r_{Q,Q}]$ and:

$R_{q,m'}$: random variable representing the number of photons in slot m' at receiver q.

$r_{q,m'}$: actual number of photons detected in the m'-th PPM slot m at q-th receiver aperture.

$I_{p,q}$: irradiance from transmitter p to receiver q.

Equation (3.2) can be developed as:

$$\widehat{m} = arg\ max_{m=1,..M} \prod_{q=1}^{Q} \prod_{m=1}^{M} \Pr\left(R_{\,q,m'} = r_{q,m'} \middle| m\right) \tag{3.3}$$

Replacing the parameters of (3.1) in (3.3) while taking into consideration that the random variables follow the Poisson distribution as stated in section 2.3, we get:

$$\widehat{m} = arg\ max_{m=1,..M} \prod_{q=1}^{Q} \left[\frac{1}{r_{q,m!}} e^{-\frac{\sum_{p=1}^{P} I_{p,q}}{P} \lambda_s - \lambda_b} \left(\frac{\sum_{p=1}^{P} I_{p,q}}{P} \lambda_s + \lambda_b \right)^{r_{q,m}} \prod_{\substack{m'=1 \\ m' \neq m}}^{M} \frac{e^{-\lambda_b} \lambda_b{}^{r_{q,m'}}}{r_{q,m'!}} \right] \tag{3.4}$$

Which can be further simplified as:

$$\widehat{m} = \arg max_{m=1,..M} \prod_{q=1}^{Q} \left[e^{-\frac{\lambda_s}{P} \sum_{p=1}^{P} I_{p,q}} \left(1 + \frac{\lambda_s}{P\lambda_b} \sum_{p=1}^{P} I_{p,q} \right)^{r_{q,m}} \prod_{m'=1}^{M} \frac{e^{-\lambda_b} \lambda_b{}^{r_{q,m'}}}{r_{q,m'!}} \right] \tag{3.5}$$

The term $e^{-\frac{\lambda_s}{P} \sum_{p=1}^{P} I_{p,q}} \prod_{m'=1}^{M} \frac{e^{-\lambda_b} \lambda_b{}^{r_{q,m'}}}{r_{q,m!}}$ can be removed since it is not dependent on m. Consequently, removing this term and taking the logarithm of the quantity in (3.5) yields:

$$\widehat{m} = arg\ max_{m=1,..M} \log \prod_{q=1}^{Q} \left[\left(1 + \frac{\lambda_s}{P\lambda_b} \sum_{p=1}^{P} I_{p,q} \right)^{r_{q,m}} \right] \tag{3.6}$$

Since log of products is equal to sum of log,

$$\widehat{m} = arg\ max_{m=1,..M} \sum_{q=1}^{Q} \log \left(1 + \frac{\lambda_s}{P\lambda_b} \sum_{p=1}^{P} I_{p,q} \right)^{r_{q,m}} \tag{3.7}$$

Since the exponent of the log is the multiplication of the exponent with the log, then the ML decoding rule is given by:

$$\hat{m} = arg\ max_{m=1,\dots M} \sum_{q=1}^{Q} r_{q,m} \log\left(1 + \frac{\lambda_s}{P\lambda_b} \sum_{p=1}^{P} I_{p,q}\right) \tag{3.8}$$

where the last equation cannot be simplified any further since the term multiplying $r_{q,m}$ depends on the receiver aperture index q.

On the other hand, a simpler implementation of the ML decoder corresponds to the EGC decoder where the decision rule takes the following simple form:

$$\hat{m} = \arg max_{m=1,..M} \left\{ \sum_{q=1}^{Q} r_{q,m} \right\} \tag{3.9}$$

This implies that the EGC decoder decides in favor of the PPM slot that has the highest photon count. In this context, the q-dependent variable weights in (3.8) are replaced by constant weights in (3.9).

3.1.2 Data rate analysis

When associated with M-PPM, the RC scheme transmits at the rate of $\log_2(M)$ bits per channel use (bpcu). This follows from the fact that the same M-PPM symbols is transmitted from all transmit apertures implying no improvement in the data rate compared to single-aperture systems.

3.1.3 Channel state information requirements

From (3.12), it follows that the implementation of the ML decoder with RC can be realized without the need to estimate any of the parameters I_1,…, I_P, λ_s, and λ_b. In this case, the decision is based solely on the numbers of photons detected in the different PPM slots without the need to estimate any of the channel parameters. This is comparable to the single aperture IM/DD FSO systems that can be implemented in the absence of CSI at the receiver. This constitutes a major advantage of the RC scheme.

3.1.4 ML decoder complexity

In this subsection, we evaluate the complexity of the ML decoders when associated with RC. The decoder's complexity will be evaluated in terms of the number of required addition operations, multiplication operations, and comparison operations. We also differentiate between symbol operations and block-operations. The first type of operations needs to be carried out on a symbol-by-symbol basis while the second type needs to be evaluated only once per fading block. In other words, the second type is not linked to any symbol statistics and it depends only on the channel values that remain the same for the time span of one block duration.

Based on equation (3.9) and in case of one receiver $Q = 1$, the ML decoder of the RC scheme requires only to compare the number of photons on each slot in order to determine the slot with the maximum value. For that and talking on the M symbol terms, we will need M comparisons among the M decision metrics without any addition or multiplication.

However, when talking in block terms, there is no need for any evaluation since the optical decision doesn't require any calculation of the parameters that depend on I_p , λ_s, and λ_b.

As for the case of Q receivers and based on equation (3.8), in addition to the M comparisons, the ML decision is made by adding the number of photons in the slots with the same position of each receiver. For that and since there are M slots, the optimal decision requires also MQ additions. Moreover, MQ multiplications are needed in order to multiply the decision variables $r_{q,m}$ by their corresponding weights.

As for the EGC decoder with Q receiver apertures, equation (3.9) shows that no multiplication operations are involved. Simply, MQ additions and M comparisons are needed to implement the decoder in this case.

When talking in block terms and for the case of ML decoder, equation (3.8) implies that P block terms need to be evaluated, namely the value $\left\{\log\left(1+\right.\right.$

$\frac{\lambda_s}{P\lambda_b}\sum_{p=1}^{P} I_{p,q}\Big)\Big\}_{p=1}^{P}$ must be calculated once per fading block. Evaluating this term requires P additions to compute $\sum_{p=1}^{P} I_{p,q}$ and P multiplications to compute $\frac{\lambda_s}{P\lambda_b}\sum_{p=1}^{P} I_{p,q}$.

As for the EGC decoder, equation (3.9) doesn't require any calculation of the parameters that depend on I_p , λ_s, and λ_b. For that, there is no block-terms to be evaluated.

Tables 1 & 2 summarize all above explanation.

Table 1 Symbol terms for RC Scheme

	Additions	Multiplication	Comparison
ML RC Q=1	0	0	M
EGC RC for All Q	MQ	0	M
ML RC for All Q	MQ	MQ	M

Table 2 Block terms for RC scheme

	Additions	Multiplication	Comparison
ML RC Q=1	0	0	0
EGC RC for All Q	0	0	0
ML RC for All Q	P	P	0

3.2 Optical Spatial Modulation (OSM)

3.2.1 Derivation of ML decoder for MISO and MIMO systems

Under the assumption that the PPM symbols m∈{1,…,M} has been transmitted, and following from sections 1.9.2 and 2.3, the parameters of the M decision variables are given by:

$$\mathrm{E}\,[R_{q,m'}] = \begin{cases} I_{p,q}\lambda_s + \lambda_b & m' = m \\ \lambda_b & m' \neq m \end{cases} \tag{3.10}$$

The ML decoder decides in favor of symbol $(\hat{p}, \hat{m})$ as per below equation

$$(\hat{p}, \hat{m}) = \arg max_{p=1,\dots,P\,;\, m=1,\dots,M} \Pr(R = r \,|p, m) \tag{3.11}$$

Where $R = \left[R_{1,1} \dots R_{1,M} \dots\dots R_{Q,1} \dots R_{Q,Q}\right]$, $r = \left[r_{1,1} \dots r_{1,M} \dots\dots r_{Q,1} \dots r_{Q,Q}\right]$ and:

$R_{q,m'}$: random variable representing the number of photons in slot m' at receiver q.

$r_{q,m'}$: actual number of photons detected in the m'-th PPM slot at q-th receiver aperture.

$I_{p,q}$: irradiance from transmitter p to receiver q.

Equation (3.11) can be developed as:

$$(\hat{p}, \hat{m}) = \arg max_{p=1,\dots,P\,;\, m=1,\dots,M} \prod_{q=1}^{Q} \prod_{m=1}^{M} \Pr\left(R_{\,q,m'} = r_{q,m'} \middle| p, m\right) \tag{3.12}$$

Replacing the parameters of (3.10) in (3.12) while taking into consideration that the random variables follow the Poisson distribution as stated in section 2.3, we get:

$$(\hat{p}, \hat{m}) = \arg max_{p=1,\dots,P\,;\, m=1,\dots,M} \prod_{q=1}^{Q} \left[\frac{e^{-(I_{p,q}\,\lambda_s+\lambda_p)} \left(I_{p,q}\,\lambda_s + \lambda_p\right)^{r_{q,m}}}{r_{q,m}!} \prod_{\substack{m'=1 \\ m' \neq m}}^{M} \frac{e^{-\lambda_b} {\lambda_b}^{r_{q,m'}}}{r_{q,m'}!} \right] \quad (3.13)$$

Which can be further simplified as:

$$(\hat{p}, \hat{m}) = \arg max_{p=1,\dots,P\,;\, m=1,\dots,M} \prod_{q=1}^{Q} \left[e^{-I_{p,q}\,\lambda_s} \left(1 + \frac{I_{p,q}\lambda_s}{\lambda_b}\right)^{r_{q,m}} \prod_{m'=1}^{M} \frac{e^{-\lambda_b} {\lambda_b}^{r_{q,m'}}}{r_{q,m}!} \right] \quad (3.14)$$

The term $\prod_{m'=1}^{M} \frac{e^{-\lambda_b} {\lambda_b}^{r_{q,m'}}}{r_{q,m!}}$ can be removed since it is not dependent on m nor on p. Consequently, removing this term and taking the logarithm of the quantity in (3.14) yields

$$(\hat{p}, \hat{m}) = \arg max_{p=1,\dots,P\,;\, m=1,\dots,M} \log \prod_{q=1}^{Q} \left[e^{-I_{p,q}\,\lambda_s} \left(1 + \frac{I_{p,q}\lambda_s}{\lambda_b}\right)^{r_{q,m}} \right] \quad (3.15)$$

Since log of products is equal to sum of log,

$$(\hat{p}, \hat{m}) = \arg max_{p=1,\dots,P\,;\, m=1,\dots,M} \left\{ \sum_{q=1}^{Q} \left(r_{q,m} \log\left(1 + \frac{I_{p,q}\lambda_s}{\lambda_b}\right) - I_{p,q}\lambda_s \right) \right\} \quad (3.16)$$

For a fixed value of p, the decision metric associated with (m', p) is greater than that associated with (m'', p) if $r_{q,m'} > r_{q,m''}$ implying that the decision rule in (3.16) can be broken down into two simpler rules as follows:

$$\widehat{m} = arg\, max_{m=1,..M} \left\{ \sum_{q=1}^{Q} r_{q,m} \log\left(1 + \frac{I_{p,q}\lambda_s}{\lambda_b}\right) \right\} \tag{3.17}$$

$$\hat{p} = arg\, max_{p=1,..P} \left\{ \sum_{q=1}^{Q} \left(r_{q,\widehat{m}} \log\left(1 + \frac{I_{p,q}\lambda_s}{\lambda_b}\right) - I_{p,q}\lambda_s \right) \right\} \tag{3.18}$$

Where $r_{q,\widehat{m}}$ is the actual number of photons in the maximum slot $\widehat{m}$ at receiver q. Similar simplifications as the ones carried out on the case of RC imply that (3.17) can be simplified as follows:

$$\widehat{m} = \arg max_{m=1,..M} \left\{ \sum_{q=1}^{Q} r_{q,m} \right\} \tag{3.19}$$

While the index of the pulsed aperture can be determined from (3.18).

3.2.2 Data rate analysis

When associated with M-PPM, the OSM scheme transmits at the rate of $\log_2(PM)$ bits per channel use (bpcu). This follows from the fact that the OSM scheme is based on pulsing only one transmit aperture per symbol duration implying there is an improvement in the data rate compared to single-aperture systems ($\log_2(M)$).

3.2.3 Channel state information requirements

It follows that the implementation of the ML decoder with OSM can be realized with the need to estimate the parameters $I_1, \dots, I_{\mathrm{p}}$, λ_s and λ_b in order to find the index of the pulsed aperture in equation (3.18).

3.2.4 ML decoder complexity

Based on equation (3.19) and in case of one receiver $Q = 1$, the ML decoder of the RC scheme requires only to compare the number of photons on each slot in order to determine the slot with the maximum value $r_{\hat{m}}$. For that and for the M symbol terms, we will need M comparisons among the M decision metrics without any addition or multiplication.

In equation (3.18) and in order to determine the index of the pulsed aperture of the maximum slot, we need to do P additions in $\left(1 + \frac{I_p \lambda_s}{\lambda_b}\right)$, P multiplications in $I_p \lambda_s$ and P comparisons among the metrics of the P apertures.

In total, for implementing both equations, we will need M + P comparisons, P additions, and P multiplications.

In case of Q receivers and similar to RC scheme, the ML decision is made by adding the number of photons on the slots with the same position of each receiver. For that and since there are M slots, the optimal decision requires additional MQ additions to the previous results of $Q = 1$ case.

However, when talking in block terms, there is no need for any evaluation in equation (3.19) since the optical decision doesn't require any calculation of the parameters that depend on I_p, λ_s, and λ_b.

On the other hand, equation (3.19) implies that $2P$ block terms need to be evaluated, namely the value $\left\{\log\left(1+\frac{\lambda_s}{P\lambda_b}\sum_{p=1}^{P} I_{p,q}\right), \lambda_s I_{p,q}\right\}_{p=1}^{P}$ must be calculated once per fading block. Although these terms require P additions, P multiplications, P divisions and P logarithm-operation, the complexity of the block-operations is smaller than the complexity of the symbol-operations. This is applicable in case of one receiver or in case of Q receivers.

Table 3 & 4 summarize all above results.

Table 3 Symbol terms for OSM scheme

	Additions	Multiplication	Comparison
ML OSM Q=1	P	P	M + P
ML OSM All Q	P+MQ	PQ	M + P

Table 4 Block terms for OSM Scheme

	Additions	Multiplication	Comparison
ML OSM Q=1	P	P	0
ML OSM All Q	P	P	0

3.3 Spatial Multiplexing (SMux)

3.3.1 Derivation of ML decoder for MIMO systems

Following from section 1.9.3, and for simplicity reasons, we consider the cases of $P = 2$ and $P = 3$ with 1 receiver. In fact, the derivations for an arbitrary value of P turned out to be very tedious.

For $P = 2$, denote by $(m_1, m_2)\ \epsilon \{1, \dots, M\}^2$ the positions of the pulses transmitted from apertures1 and 2. The decision metric varies depending on whether $m_1 = m_2$ or $m_1 \neq m_2$.

If $\boldsymbol{m_1 = m_2}$

The parameters of the M decision variables are given by:

$$\mathrm{E}\,[R_{m'}] = \begin{cases} \dfrac{I_1 + I_2}{2}\lambda_s + \lambda_b & m' = m \\ \lambda_b & m' \neq m \end{cases} \tag{3.20}$$

In this case, the decision metric is similar to the case of RC scheme with one receiver. In fact, in this special case, the same PPM symbol m is transmitted from the two transmit apertures.

The same derivation of section 3.1.1 will apply. Taking the algorithm of equation (3.4) and removing the last term that does not depend on m, we end up with the following decision metric:

$$\log\left[e^{-\left(\frac{(I_1+I_2)\lambda_s}{2}\right)}\ \left(1 + \frac{\lambda_s}{2\lambda_b}(I_1 + I_2)\right)^{r_m}\right] \tag{3.21}$$

Since log of products is equal to sum of log,

$$r_m \log\left(1 + \frac{\lambda_s}{P\lambda_b}\sum_{p=1}^{P} I_p\right) - \frac{(I_1 + I_2)\lambda_s}{2} \tag{3.22}$$

If $\boldsymbol{m_1 \neq m_2}$

The decision metric is given by:

$$r_m \log\left(1 + \frac{\lambda_s}{P\lambda_b}\sum_{p=1}^{P} I_{p,}\right) \prod_{\substack{m'=1 \\ m' \neq m_1 \\ m' \neq m_2}}^{M} \frac{e^{-\lambda_b}{\lambda_b}^{r_{m'}}}{r_{m'!}} \tag{3.23}$$

The terms in (3.23) can be arranged as follows:

$$\left[e^{-\frac{I_1\lambda_s}{2}}\left(1 + \frac{I_1\lambda_s}{2\lambda_b}\right)^{r_{m_1}} \times e^{-\frac{I_2\lambda_s}{2}}\left(1 + \frac{I_2\lambda_s}{2\lambda_b}\right)^{r_{m_2}}\right] \times \prod_{m'=1}^{M} \frac{e^{-\lambda_b}{\lambda_b}^{r_{m'}}}{r_{m'}!} \tag{3.24}$$

$\prod_{m'=1}^{M} \frac{e^{-\lambda_b}{\lambda_b}^{r_{m'}}}{r_{m'!}}$ can be removed since it is not dependent on m. Consequently, the log of the decision metric in (3.24) simplifies to:

$$\log\left[e^{-\frac{I_1\lambda_s}{2}}\left(1 + \frac{I_1\lambda_s}{2\lambda_b}\right)^{r_{m_1}} \times e^{-\frac{I_2\lambda_s}{2}}\left(1 + \frac{I_2\lambda_s}{2\lambda_b}\right)^{r_{m_2}}\right] \tag{3.25}$$

Since Log of products is equal to the sum of Log and since the exponent of the Log is the multiplication of the exponent with the Log, we get the following generalized formula for the decision metric:

$$\left(r_{m_1}\log\left(1+\frac{I_1\lambda_s}{2\lambda_b}\right)+r_{m_2}\log\left(1+\frac{I_2\lambda_s}{2\lambda_b}\right)-\frac{I_1+I_2}{2}\lambda_s\right) \tag{3.26}$$

Now, comparing (3.22) and (3.26) shows that the term $-\frac{I_1+I_2}{2}\lambda_s$ appears in both equations. Therefore, this term can be ignored since it doesn't not affect the selection of the decision metric with maximum value.

Therefore, from equations (3.22) and (3.26), the ML decision rule with $P=2$ transmit apertures and $Q=1$ receive aperture can be expressed by:

$$(\hat{m}_1,\hat{m}_2)=\ arg\,max_{(m_1,m_2)\,\epsilon\,\{1,\ldots,M\}^2}\ \{W_{m_1,m_2}\} \tag{3.27}$$

Where

$$W_{m_1,m_2}=\begin{cases} r_m\alpha_{1,2} & m_1=\ m_2=m \\ r_{m_1}\alpha_1+r_{m_2}\alpha_2 & m_1\neq m_2 \end{cases} \tag{3.28}$$

With

$$\alpha_i=\log\left(1+\ \frac{\lambda_s}{2\lambda_b}\ I_i\right);\quad i=1,2. \tag{3.29}$$

$$\alpha_{1,2}=\log\left(1+\ \frac{\lambda_s}{2\lambda_b}\ (I_1+I_2)\right) \tag{3.30}$$

From (3.28), the metric $r_m\alpha_{1,2}$ is maximized when $r_m$is maximized.

In the same way, $r_{m_1}\alpha_1+r_{m_2}\alpha_2$ is maximized if slots m_1 and m_2 result in the maximum counts with $r_{m_1}>r_{m_2}$ if $\alpha_1>\ \alpha_2$ and $r_{m_1}<\ r_{m_2}$ if $\alpha_1<\ \alpha_2$. Note that α_1 is an increasing function of I_1 while α_2 is an increasing function of I_2.

Based on that, we can simplify the SMux procedure by defining the following two positions:

$$\hat{m} = arg\,max_{m=1,\dots,M}\{r_m\} \quad ; \hat{m}' = arg\,max_{\substack{m=1,\dots,M \\ m\neq\hat{m}}}\{r_m\} \tag{3.31}$$

Where $\hat{m}$ is the slot with the maximum count and $\hat{m}'$ is the second highest count. Based on this definition, the ML decoder decides in favor of:

$$(\hat{m},\hat{m}') \tag{3.32}$$
$$= \begin{cases} (\hat{m},\hat{m}) & condition\ 1\ is\ satisfied \\ (\hat{m},\hat{m}') & condition\ 1\ is\ not\ \ satisfied\ and\ I_1 > I_2 \end{cases}$$

Where condition 1 is defined as:

$$r_{\hat{m}}\,\alpha_{1,2} > r_{\hat{m}}\,\max\{\alpha_1,\alpha_2\} + r_{\hat{m}'}\,\min\{\alpha_1,\alpha_2\} \tag{3.33}$$

For $P = 3$, denote by $(m_1, m_2, m_3) \in \{1,\dots,M\}^2$ the positions of the pulses transmitted from apertures1, 2 and 3. The decision metric varies based on whether

$m_1 = m_2 = m_3$ (referred to case 1) or the 3 positions are not all the same (referred to as case 2).

Case 1: $m_1 = m_2 = m_3 = m$

The parameters of the M decision variables are given by:

$$\mathrm{E}\,[R_{m'}] = \begin{cases} \dfrac{I_1 + I_2 + I_3}{3}\lambda_s + \lambda_b & m' = m \\ \lambda_b & m' \neq m \end{cases} \tag{3.34}$$

In this case, the decision metric is similar to the case of RC scheme with one receiver. In fact, in this special case, the same PPM symbol m is transmitted from all three transmit apertures.

The same derivation of section 3.1.1 will apply. Taking the algorithm of equation (3.4) and removing the last term that does not depend on m, we end up with the following decision metric (with $Q = 1$):

$$\log\left[e^{-\left(\frac{(I_1+I_2+I_3)\lambda_s}{3}\right)}\left(1+\frac{\lambda_s}{3\lambda_b}(I_1+I_2+I_3)\right)^{r_m}\right] \tag{3.35}$$

That simplifies to

$$r_m \log\left(1+\frac{\lambda_s}{3\lambda_b}(I_1+I_2+I_3)\right)-\frac{(I_1+I_2+I_3)\lambda_s}{3} \tag{3.36}$$

Case 2:

This case comprises the following subcases.

Case 2.1: $m_1 \neq m_2 \neq m_3$

In this case, the decision metric is given by:

$$\left[\frac{e^{-\left(\frac{I_1\lambda_s}{3}+\lambda_b\right)}\left(\frac{I_1\lambda_s}{3}+\lambda_b\right)^{r_{m_1}}}{r_{m_1}!}\times\frac{e^{-\left(\frac{I_2\lambda_s}{3}+\lambda_b\right)}\left(\frac{I_2\lambda_s}{3}+\lambda_b\right)^{r_{m_2}}}{r_{m_2}!}\times\frac{e^{-\left(\frac{I_3\lambda_s}{3}+\lambda_b\right)}\left(\frac{I_2\lambda_s}{3}+\lambda_b\right)^{r_{m_3}}}{r_{m_3}!}\right]\prod_{\substack{m'=1\\ m'\neq m_1\\ m'\neq m_2\\ m'\neq m_3}}^{M}\frac{e^{-\lambda_b}\lambda_b{}^{r_{m'}}}{r_{m'}!} \tag{3.37}$$

Which can be further simplified to the following:

$$\left[e^{-\frac{I_1\lambda_s}{3}}\left(1+\frac{I_1\lambda_s}{3\lambda_b}\right)^{r_{m_1}}\times e^{-\frac{I_2\lambda_s}{3}}\left(1+\frac{I_2\lambda_s}{3\lambda_b}\right)^{r_{m_2}}\times e^{-\frac{I_3\lambda_s}{3}}\left(1+\frac{I_3\lambda_s}{3\lambda_b}\right)^{r_{m_3}}\right]\times\prod_{m'=1}^{M}\frac{e^{-\lambda_b}\lambda_b{}^{r_{m'}}}{r_{m'}!} \quad (3.38)$$

The term $\prod_{m'=1}^{M}\frac{e^{-\lambda_b}\lambda_b{}^{r_{m'}}}{r_{m'}!}$ can be removed since it is not dependent on m. Therefore, the log of (3.38) simplifies to:

$$\log\left[e^{-\frac{I_1\lambda_s}{3}}\left(1+\frac{I_1\lambda_s}{3\lambda_b}\right)^{r_{m_1}}\times e^{-\frac{I_2\lambda_s}{3}}\left(1+\frac{I_2\lambda_s}{3\lambda_b}\right)^{r_{m_2}}\times e^{-\frac{I_3\lambda_s}{3}}\left(1+\frac{I_3\lambda_s}{3\lambda_b}\right)^{r_{m_3}}\right] \quad (3.39)$$

Since Log of products is equal to the sum of Log and since the exponent of the Log is the multiplication of the exponent with the Log, we get the following generalized formula for the decision metric:

$$r_{m_1}\log\left(1+\frac{I_1\lambda_s}{3\lambda_b}\right)+r_{m_2}\log\left(1+\frac{I_2\lambda_s}{3\lambda_b}\right)+\ r_{m_3}\log\left(1+\frac{I_3\lambda_s}{3\lambda_b}\right)-\frac{I_1+I_2+I_3}{3}\lambda_s \quad (3.40)$$

Where the term $-\frac{I_1+I_2+I_3}{3}\lambda_s$ can be ignored since it doesn't depend on m and since it will appear in all consequent decision metrics as will be shown later.

Case 2.2: $m_1 = m_2$, $m_1 \neq m_3$

The decision metric in this case is given by:

$$\left[\frac{e^{-\left(\frac{(I_1+I_2)\lambda_s}{3}+\lambda_b\right)}\left(\frac{(I_1+I_2)\lambda_s}{3}+\ \lambda_b\right)^{r_m}}{r_m!}\times\frac{e^{-\left(\frac{I_3\lambda_s}{3}+\lambda_b\right)}\left(\frac{I_2\lambda_s}{3}+\lambda_b\right)^{r_{m_3}}}{r_{m_3}!}\right]\prod_{\substack{m'=1\\ m'\neq m\\ m'\neq m_3}}^{M}\frac{e^{-\lambda_b}\lambda_b{}^{r_{m'}}}{r_{m'}!} \quad (3.41)$$

Where $m = m_1 = m_2$

(3.41) can be further simplified to the following:

$$\left[e^{-\frac{(I_1+I_2)\lambda_s}{3}}\left(1+\frac{(I_1+I_2)\lambda_s}{3\lambda_b}\right)^{r_m}\times e^{-\frac{I_3\lambda_s}{3}}\left(1+\frac{I_3\lambda_s}{3\lambda_b}\right)^{r_{m_3}}\right]\times\prod_{m'=1}^{M}\frac{e^{-\lambda_b}{\lambda_b}^{r_{m'}}}{r_{m'}!} \tag{3.42}$$

$\prod_{m'=1}^{M}\frac{e^{-\lambda_b}{\lambda_b}^{r_{m'}}}{r_{m'}!}$ Can be removed since it is not dependent on m.

$$\log\left[e^{-\frac{(I_1+I_2)\lambda_s}{3}}\left(1+\frac{(I_1+I_2)\lambda_s}{3\lambda_b}\right)^{r_m}\times e^{-\frac{I_3\lambda_s}{3}}\left(1+\frac{I_3\lambda_s}{3\lambda_b}\right)^{r_{m_3}}\right] \tag{3.43}$$

Since Log of products is equal to the sum of Log and since the exponent of the Log is the multiplication of the exponent with the Log, we get the following generalized formula for the decision metric:

$$r_m\log\left(1+\frac{(I_1+I_2)\lambda_s}{3\lambda_b}\right)+r_{m_3}\log\left(1+\frac{I_3\lambda_s}{3\lambda_b}\right)-\frac{I_1+I_2+I_3}{3}\lambda_s \tag{3.44}$$

Where the term $-\frac{I_1+I_2+I_3}{3}\lambda_s$ can be ignored since it doesn't depend on m.

The same derivation applies on cases $\boldsymbol{m_1 \neq m_2}$, $\boldsymbol{m_1 = m_3 = m}$ to get the following decision metric

$$r_m\log\left(1+\frac{(I_1+I_3)\lambda_s}{3\lambda_b}\right)+r_{m_2}\log\left(1+\frac{I_2\lambda_s}{3\lambda_b}\right)-\frac{I_1+I_2+I_3}{3}\lambda_s \tag{3.45}$$

And for $\boldsymbol{m_1 \neq m_2}$, $\boldsymbol{m_2 = m_3 = m}$ to get the following decision metric

$$r_m \log\left(1+\frac{(I_2+I_3)\lambda_s}{3\lambda_b}\right)+r_{m_1}\log\left(1+\frac{I_1\lambda_s}{3\lambda_b}\right)-\frac{I_1+I_2+I_3}{3}\lambda_s \tag{3.46}$$

Following from equations (3.36), (3.40), (3.44), (3.45) and (3.46), the ML SMux decision rule can be expressed by

$$(\hat{m}_1,\hat{m}_2,\hat{m}_3) = \ arg\,max_{(m_1,m_2,m_3)\,\epsilon\,\{1,\ldots,M\}^3}\ \{w_{m_1,m_2,m_3}\} \tag{3.47}$$

Where

$$W_{m_1,m_2,m_3} = \begin{cases} r_m\alpha_{1,2,3} & m_1 = m_2 = m_3 = m \\ r_{m_1}\alpha_1 + r_{m_2}\alpha_2 + r_{m_3}\alpha_3 & m_1 \neq m_2 \neq m_3 \\ r_m\alpha_{12} + r_{m_3}\alpha_3 & m_1 = m_2 = m\,, m_1 \neq m_3 \\ r_m\alpha_{13} + r_{m_2}\alpha_2 & m_1 \neq m_2\,, m_1 = m_3 = m \\ r_m\alpha_{23} + r_{m_1}\alpha_1 & m_1 \neq m_2\,, m_2 = m_3 = m \end{cases} \tag{3.48}$$

With

$$\alpha_i = \log\left(1+\frac{\lambda_s}{3\lambda_b}\,I_i\right);\quad i=1,2,3. \tag{3.49}$$

$$\alpha_{1,2} = \log\left(1+\frac{\lambda_s}{3\lambda_b}\,(I_1+I_2)\right) \tag{3.50}$$

$$\alpha_{2,3} = \log\left(1+\frac{\lambda_s}{3\lambda_b}\,(I_2+I_3)\right) \tag{3.51}$$

$$\alpha_{1,3} = \log\left(1+\frac{\lambda_s}{3\lambda_b}\,(I_1+I_3)\right) \tag{3.52}$$

$$\alpha_{1,2,3} = \log\left(1+\frac{\lambda_s}{3\lambda_b}\,(I_1+I_2+I_3)\right) \tag{3.53}$$

3.3.2 Data rate analysis

When associated with M-PPM, the SMux scheme transmits at the rate of $P \log_2 M$ bits per channel use (bpcu). This follows from the fact that independent data streams are transmitted from the P transmit apertures in the SMux scheme implying that there is a P-fold improvement in the data rate compared to single-aperture systems.

3.3.3 Channel state information requirements

It follows that the implementation of the ML decoder with SMux can be realized with the need to estimate the parameters I_1, I_2, λ_s and λ_b in order to calculate equation (3.29) in the case of $P = 2$ and to estimate the parameters I_1, I_2, I_3, λ_s and λ_b in order to calculate equation (3.49) in the case of P = 3.

3.3.4 ML decoder complexity

To be able to find the decoder complexity of the SMux scheme with $P = 2$ case, we analyze equation (3.33) and check the number of additions, multiplications and comparisons needed.

There is one multiplication in $m_1 = m_2$ case to get the value of $r_m \alpha_{1,2}$.

In the case of $m_1 \neq m_2$, there are two multiplications and one addition to getting $r_{\widehat{m}} \max\{\alpha_1, \alpha_2\} + r_{\widehat{m}'} \min\{\alpha_1, \alpha_2\}$.

As for the comparison, equation (3.31) requires M comparisons to get $\widehat{m}$ and $M - 1$ comparisons are needed to find $\widehat{m}'$ since out of the M symbols the maximum slot has already been found.

Moreover, equations (3.33) requires one comparison to find $condition\ 1$ and evaluate which case of equation (3.32) is the right case.

Based on that, we can summarize the ML decoder complexity of the SMux scheme with $P = 2$ as per the following table

Table 5 Symbol terms for SMux (2x1) scheme

	Additions	Multiplication	Comparison
ML SMux 2 x 1 Second decoder	1	3	2M

To be able to find the decoder complexity of the SMux scheme with $P = 3$ case, we analyze equation (3.48) and check the number of additions, multiplications and comparisons needed for each of the five following cases.

Case 1: $\boldsymbol{m_1 = m_2 = m_3 = m}$

Evaluating the term $r_m \alpha_{1,2,3}$ in equation (3.48) requires one multiplication and no addition. Since the three apertures will transmit in the same slot out of the M slots symbol, this means that we have M possibilities. Multiplying the number of terms by the number of additions and multiplications, we end up with M multiplications and no addition for this case.

Case 2: $\boldsymbol{m_1 \neq m_2 \neq m_3}$

This is the case where each of the three apertures transmit in a separate slot out of the M slots. The first aperture can pick and transmit in any of the M slots, the second aperture will have to pick one of the remaining slots which means pick one of the $M - 1$ slots and in the same sense the third aperture will have to pick one out of the $M - 2$ slots to transmit. Thus, the number of the terms for this case will be $M(M-1)(M-2)$ terms.

Moreover, each term requires 3 multiplications and 2 additions to evaluate the term $r_{m_1}\alpha_1 + r_{m_2}\alpha_2 + r_{m_3}\alpha_3$ in equation (3.48) . Multiplying the number of terms by the number of additions and multiplications, we end up with $3M(M-1)(M-2)$ multiplications and $2M(M-1)(M-2)$ additions for this case.

Cases 3 to 5:

The remaining three cases have the same scenario where two of the three apertures will transmit in the same slot out of the M slots and the third aperture will transmit in one of the remaining $M-1$ slots. Thus, the number of terms of each of these cases is $M(M-1)$ terms.

Moreover, each term requires 2 multiplications and 1 addition to evaluate any of the three terms $r_m\alpha_{12} + r_{m_3}\alpha_3$ or $r_m\alpha_{13} + r_{m_2}\alpha_2$ or $r_m\alpha_{23} + r_{m_1}\alpha_1$of equation (3.48). Multiplying the number of terms by the number of additions and multiplications, we end up with $2M(M-1)$ multiplications and $M(M-1)$ additions for each case.

To evaluate the complexity of the $3x1$ SMux decoder, we will have to add the number of additions for each case to find the total number of additions required, The same applies for the total number of multiplications.

Total number of additions $= 0 + 2M(M-1)(M-2) + \big(3\ x\ M(M-1)\big)$

$$= 2M^3 - 3M^2 + M$$

Total number of multiplications $= M + 3M(M-1)(M-2) + \big(3\ x\ 2M(M-1)\big)$

$$= 3M^3 - 3M^2 + M$$

Total number of comparisons $= M^3$

Where the total number of comparisons corresponds to the total number of SMux symbols.

Table 6 below summarizes all above explanations

Table 6 Symbol terms for SMux (3x1) scheme

Cases	*Number of Addition per term*	*Number of Multiplication per term*	*Number of terms*
Case 1	0	*1*	$3M$
Case 2	*2*	*3*	$M(M-1)(M-2)$
Case 3	*1*	*2*	$M(M-1)$
Case 4	*1*	*2*	$M(M-1)$
Case 5	*1*	*2*	$M(M-1)$

3.4 Theoretical Method of evaluating BER of OSM scheme

The general formula of the theoretical method of the BER of the OSM scheme is the following:

$$BER = P_{error,slot} + \left[\left(1 - P_{error,slot}\right) \times P_{error,aperture}\right] \tag{3.4.1}$$

Where $P_{error,slot}$ is the probability of error for the slot position of the symbol. In other words, an error occurs when the detector decides in favor of the PPM slot that doesn't have the maximum count of photons. In this case, there is no need to check if the receiver was able to guess which aperture the signal was coming from since the OSM symbol will be eventually in error.

As for the second part of the summation, the error occurs when the detector decides correctly which PPM slot has the maximum count however giving the wrong aperture number of the correspondent signal. Not to mention that $P_{error,aperture}$ is the probability of error for the index aperture.

This formula derivation is divided into the following two sections:

3.4.1 Finding $P_{error,slot}$

Following up from the same explanation in section 1.6.3 and from equation (1.3), the channel irradiances follow the gamma-gamma channel model.

For Q-PPM, the probability of error is given by:

$$P(e) = \sum_{i=1}^{Q} P(e|i)\,\Pr(i\ was\ sent) = \frac{1}{Q}\sum_{i=1}^{Q} P(e|i) = P(e|1) \tag{3.4.2}$$

The second equality follows from the assumption that the symbols are equiprobable.
The last equality follows from the symmetry of the signal set.

In the absence of background noise, an error occurs only when the electron count in each slot is equal to zero. Since when this occurs, a correct decision is made with probability $1/Q$ following from the random tie breaking (to select the max), then:

$$P(e) = \left(\frac{Q-1}{Q}\right)\Pr(N_1 = 0|1)$$

$$P(e) = \left(\frac{Q-1}{Q}\right) e^{-\lambda_s} \tag{3.4.3}$$

In the presence of background noise, it is more convenient to calculate the SER using the following relation:

$$P(e) = P(e|1) = 1 - P(c|1) \tag{3.4.4}$$

Where $P(c|1)$ is the probability of making a correct decision when symbol 1 was sent.
When i counts are equal to the maximum count, a correct decision is made with probability $1/i$. Consequently, $P(c|1)$ can be written as:

$$P(c|1) = \sum_{i=1}^{Q} \frac{1}{i} P(c|1,i) \tag{3.4.5}$$

$P(c|1,i)$ is the probability of correct decision with i ties (i counts are equal to the maximum count).

In general, the following relation is verified for all values of i:

$$P(c|1,i) = \binom{Q-1}{i-1}\Pr(N_1 = N_2, \dots, N_1 = N_i, N_1 > N_{i+1}, \dots, N_1 > N_Q|1) \quad (3.4.6)$$

Where $\binom{m}{k} = \frac{m!}{k!(m-k)!}$ is the number of possible combinations of k random variables out of the total number of m random variables.

Consequently,

$$\frac{1}{\binom{Q-1}{i-1}} P(c|1,i) = \sum_{k=0}^{+\infty} \Pr(N_1 = k|1) \prod_{j=2}^{i} \Pr(N_j = k|1) \prod_{j=i+1}^{Q} \Pr(N_j < k|1) \quad (3.4.7)$$

while taking into consideration that the random variables follow the Poisson distribution as stated in section 2.3, we get:

$$\frac{1}{\binom{Q-1}{i-1}} P(c|1,i) = \sum_{k=0}^{+\infty} \left[\frac{1}{k!} e^{-(\lambda_b + I_p\lambda_s)}(\lambda_b + I_p\lambda_s)^k\right] \left[\frac{1}{k!} e^{-\lambda_b} {\lambda_b}^k\right]^{i-1} \left[\sum_{j=0}^{k-1} \frac{1}{j!} e^{-\lambda_b} {\lambda_b}^j\right]^{Q-i} \quad (3.4.8)$$

Arranging the above equation will give:

$$P_{error,slot} = 1 - \sum_{i=1}^{Q} \frac{1}{i} \binom{Q-1}{i-1} \sum_{k=0}^{+\infty} \left[\frac{1}{k!} e^{-(\lambda_b + I_p\lambda_s)}(\lambda_b + I_p\lambda_s)^k\right] \left[\frac{1}{k!} e^{-\lambda_b} {\lambda_b}^k\right]^{i-1} \left[\sum_{j=0}^{k-1} \frac{1}{j!} e^{-\lambda_b} {\lambda_b}^j\right]^{Q-i} \quad (3.4.9)$$

3.4.2 Finding $P_{error,aperture}$

Assume that the channel irradiances are arranged in increasing order as per the following:

$$I_1 < I_2 < \cdots < I_P \tag{3.4.10}$$

This allows us to set threshold levels between two consecutive channel irradiances.

Denote by γ_p the threshold level between I_{p-1} and I_p.

We set $\gamma_1 = 0$ and $\gamma_{P+1} \to +\infty$

Taking the Poisson distribution of the channel irradiance we get the following relation for determining γ_p:

$$\frac{e^{-(I_p\lambda_s+\lambda_b)}(I_p\lambda_s+\lambda_b)^r}{r!} > \frac{e^{-(I_{p-1}\lambda_s+\lambda_b)}(I_{p-1}\lambda_s+\lambda_b)^r}{r!} \tag{3.4.11}$$

Where r is the number of photons detected.

Removing the $r!$ and taking the elements dependent on r to one side:

$$\frac{(I_p\lambda_s+\lambda_b)^r}{(I_{p-1}\lambda_s+\lambda_b)^r} > \frac{e^{-(I_{p-1}\lambda_s+\lambda_b)}}{e^{-(I_p\lambda_s+\lambda_b)}} \tag{3.4.12}$$

By taking the logarithm of both sides will allow us to remove r and by simplifying, we get:

$$r\ln\frac{(I_p\lambda_s+\lambda_b)}{(I_{p-1}\lambda_s+\lambda_b)} > (I_p - I_{p-1})\lambda_s \tag{3.4.13}$$

We get the following threshold level formula for the value of r:

$$\gamma_p = \left\lceil \frac{(I_p - I_{p-1})\lambda_s}{\ln \frac{(I_p\lambda_s + \lambda_b)}{(I_{p-1}\lambda_s + \lambda_b)}} \right\rceil \tag{3.4.14}$$

This means we are taking the threshold as a value between $I_p \; and \; I_{p-1}$.

Since the Poisson distribution is not symmetrical, γ_p can't be considered as the mean of $I_p \; and \; I_{p-1}$.

We are taking the ceil of equation (3.4.13) since we are dealing with entire numbers of photons.

In order to find the index of the pulsed aperture:

- Find the threshold levels from $p = 2, \dots, P$.
- check if r is between $[\gamma_p \quad \gamma_{p+1} - 1]$

Based on that logic, we can get the following probability of error:

$$P_{error,aperture} = 1 - \frac{1}{P}\sum_{p=1}^{P}\sum_{k=\gamma_p}^{\gamma_{p+1}-1} \frac{e^{-(I_p\lambda_s+\lambda_b)}(I_p\lambda_s + \lambda_b)^k}{k!} \tag{3.4.15}$$

3.5 Theoretical Method of evaluating BER of RC scheme

Following from the same derivation of section 3.4, the only difference between equations (3.4.9) and (3.5.1) is that instead of multiplying λ_s by each aperture channel irradiance, we multiply by the summation of the channel irradiances and we divide by the number of apertures. Therefore:

$$P_{error,slot} = 1 - \sum_{i=1}^{Q} \frac{1}{i}\binom{Q-1}{i-1} \sum_{k=0}^{+\infty} \left[\frac{1}{k!} e^{-(\lambda_b + \frac{\sum_{p=1}^{P} I_p}{P}\lambda_s)} (\lambda_b + \frac{\sum_{p=1}^{P} I_p}{P}\lambda_s)^k \right] \left[\frac{1}{k!} e^{-\lambda_b} {\lambda_b}^k \right]^{i-1} \left[\sum_{j=0}^{k-1} \frac{1}{j!} e^{-\lambda_b} {\lambda_b}^j \right]^{Q-i} \quad (3.5.1)$$

which provides the error probability of the RC scheme.

3.6 Comparison between RC, OSM and SMux

Below table summarizes the difference between all three schemes along with the ML decoder complexities that were previously explained in each previous section separately:

Table 6 Comparison of the ML decoder complexity between all three schemes

	$RC\ (P\ x\ Q)$	$OSM\ (P\ x\ Q)$	$SMux(2\ x\ 1)$	$SMux(3\ x\ 1)$
Bit Rate	$\log_2(M)\ bpcu$	$\log_2(PM)\ bpcu$	$2\log_2(M)\ bpcu$	$3\log_2(M)\ bpcu$
CSI Requirement	*No*	*Yes*	*Yes*	*Yes*
Block Terms	None	$\left\{\log\left(1+\frac{I_p\lambda_s}{\lambda_b}\right)\right\}_{p=1}^{P}$	$\{\alpha_1,\alpha_2,\alpha_{12}\}$	$\begin{Bmatrix}\alpha_1,\alpha_2,\alpha_3,\alpha_{12},\\ \alpha_{13},\alpha_{23},\alpha_{1,2,3}\end{Bmatrix}$
Comparisons (per symbol)	M	$M+P$	$2M$	M^3
Multiplications (per symbol)	MQ	PQ	3	$3M^3-3M^2+M$
Additions (per symbol)	MQ	$P+MQ$	1	$2M^3-3M^2+M$

This table shows that SMux is the most complex scheme among the compared schemes since it has the largest number of symbol-level multiplications and comparisons while RC scheme is the simplest since it has the smallest number of symbol-level multiplications and comparisons (Not to mention that addition operations are easier than multiplications and comparisons) and since it needs no channel state information compared to SMux and OSM schemes.

Based on that, the OSM scheme is considered as a compromise between the SMux and RC schemes in a matter of rate and complexity with SMux being at the high end and RC being at the lower end.

In addition to the above, all three schemes must be compared in terms of error performance. This comparison will be presented in the following section.

Chapter 4

Numerical Results

1.17 Error performance for FSO links in all studied scenarios

In this section, we show some numerical results that support the findings reported in the previous sections. In what follows, the SERs of the RC, OSM, and SMux schemes will be compared numerically based on Monte Carlo simulations. The refractive index structure constant is set to $C_n^2 = 1.7 \times 10^{-14}\, m^{-2/3}$. We also fix $\eta = 0.5$ and $\lambda = 1550\, nm$ in (2.3.1) and (2.3.2). Results show the variations of the SER as a function of the signal energy E_s per information bit where this quantity is given by $\frac{E_s}{\log_2(M)}$, $\frac{E_s}{\log_2(\mathrm{P}M)}$, and $\frac{E_s}{\mathrm{P}\log_2(M)}$, for the RC, OSM and SMux schemes, respectively. This normalization is needed since the three schemes transmit at different rates.

For all below results, the distance between the transmitter and the receiver is fixed to d=5 km. We also set $\frac{P_b T_s}{M} = -185\, dBJ$ as the background noise level.

Fig. 23 compares the different schemes for 8-PPM, 2 transmit apertures, 2 receiver apertures for $d = 5\ km$. In this case, the RC scheme transmits at a rate of 3 bpcu while OSM transmits at a rate of 4 bpcu and SMux transmits at a rate of 6 bpcu. In terms of complexity, the RC scheme requires 8 comparisons, 16 multiplications, and 16 additions. As for the OSM scheme, it requires 10 comparisons, 2 multiplications, and 18 additions and the SMux scheme requires 16 comparisons, 19 multiplications, and 17 additions. In terms of performance, the RC scheme shows the best performance compared to OSM and SMux especially for large values of the signal energy E_s. However, it's worth noting that the good performance of RC is associated by a bit rate that is the lowest among the three compared schemes. Based on what preceded, the following conclusions can be drawn from fig 23.

The RC scheme is more convenient for small rate and low complexity systems while SMux is adapted to high rate systems with bigger processing capabilities. OSM scheme can be considered as a compromise scheme between RC and SMux schemes since it has a higher bit rate than RC but lower than SMux and has lower complexity than SMux but higher than RC.

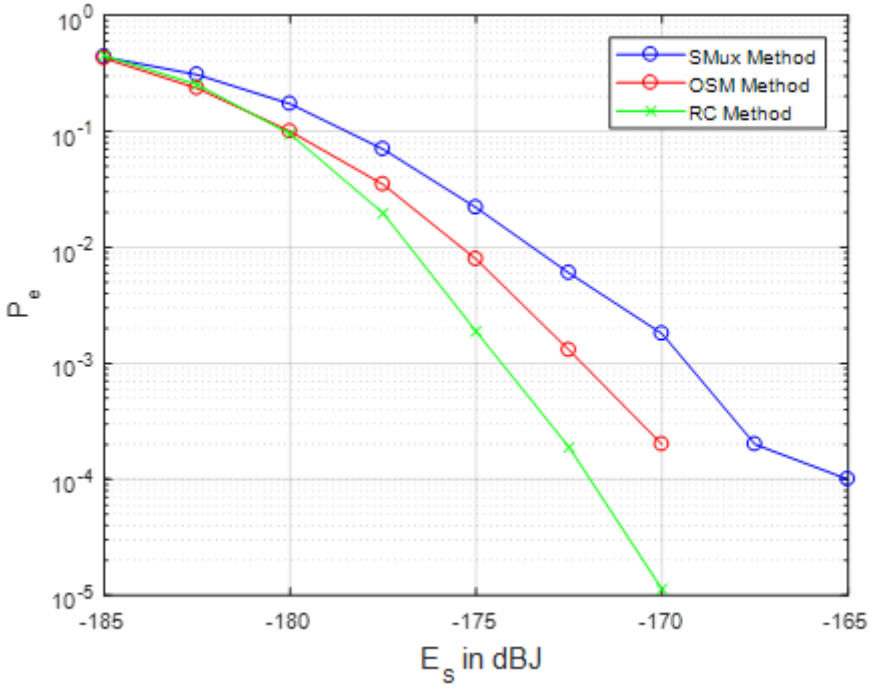

Figure 23 All three schemes for a 2 x2 System with 8-PPM

The same simulation setup is reproduced in Fig. 24 for 3x3 systems with 2-PPM. For E_s values that are smaller than -177 dBJ, the SMux scheme in Fig. 24 outperforms the OSM scheme and the opposite in case of E_s values that are larger than -177 dBJ. This means that the complexity reduction resulting from the OSM scheme is not only marginal, but it is also associated with non-negligible performance degradations especially for a large value of E_s. Comparing the performances of Fig. 24 with the ones of Fig. 25, the SER of RC and OSM schemes starts at 0.2 in case of 3x3 systems and at 0.4 in case of 2x2 systems. This means that the SER is expected to improve significantly when increasing the number of photo-detectors at the receiver.

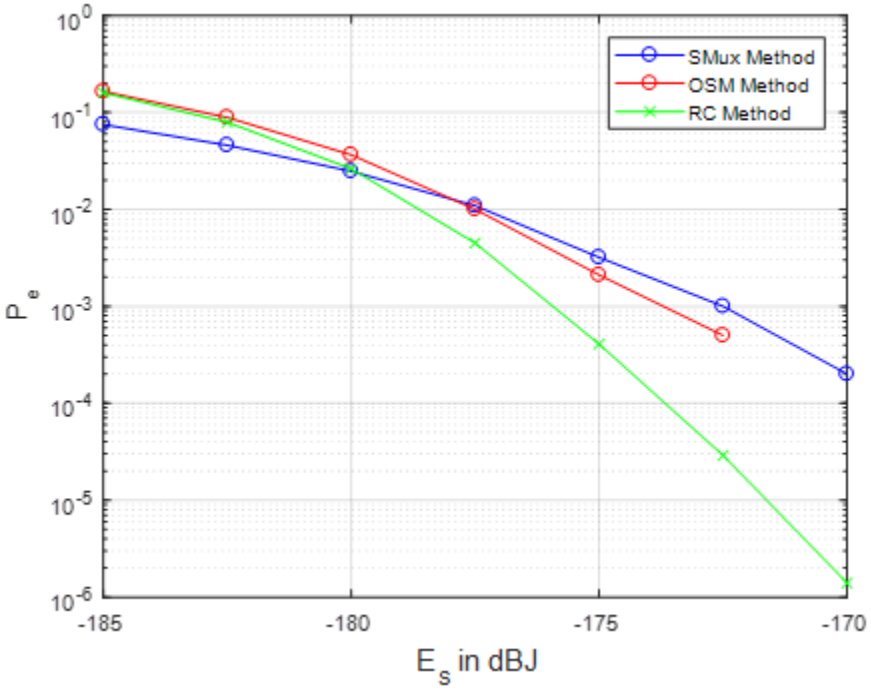

Figure 24 All three schemes for a 3 x 3 System with 2-PPM

Fig. 25 also shows the performance of 3x3 systems where the number of PPM slots is increased from 2 to 4. Comparing Fig.25 with Fig.24, the bit rates of all three schemes have increased since there is an increase of the PPM slots from 2 to 4 while keeping the same number of transmitters and receivers. The E_s value where the OSM starts to outperform the SMux scheme is at -183 dBJ instead of -177 dBJ. This indicates that at higher bit rates, the BER of OSM improves at smaller signal power.

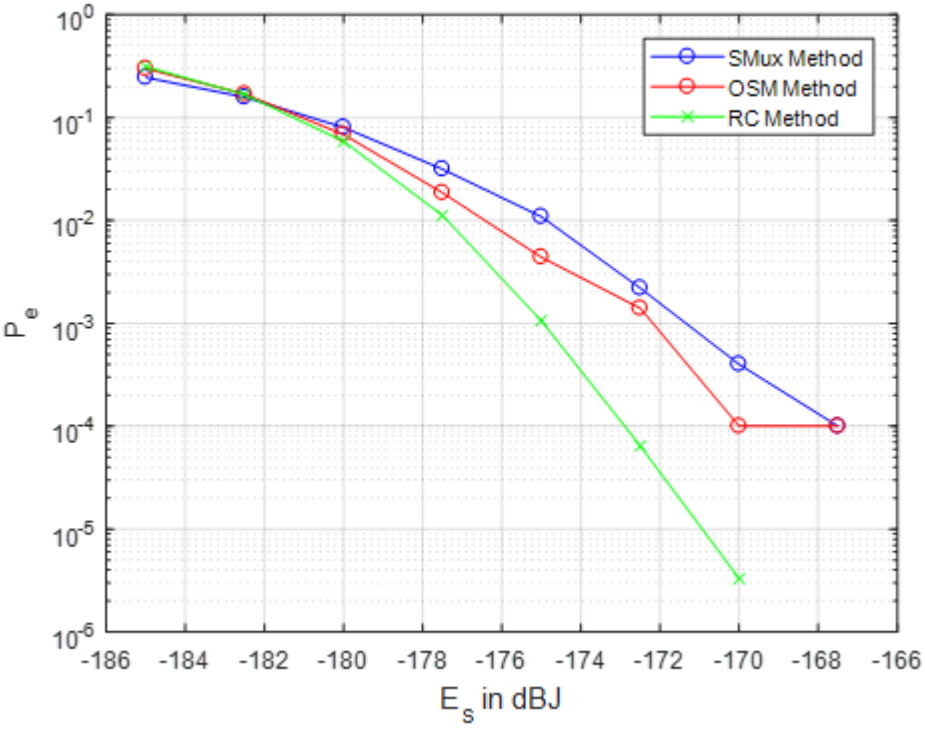

Figure 25 All three schemes for a 3 x 3 System with 4-PPM

Fig. 26 shows that the RC scheme has a better performance for a higher number of receivers. For signal energy of -180 dBJ and for $d = 5\ km$, the 1 receiver RC scheme shows a bit error rate of 0.01 which is significantly higher than the 5 receivers RC scheme that shows a bit error rate of $4.8\ x\ 10^{-6}$. This can be explained that for more receivers we can have higher accuracy for determining the slot position with the highest number of photons. In this case, the number of collected signal photons has a higher chance of exceeding the number of noise photons.

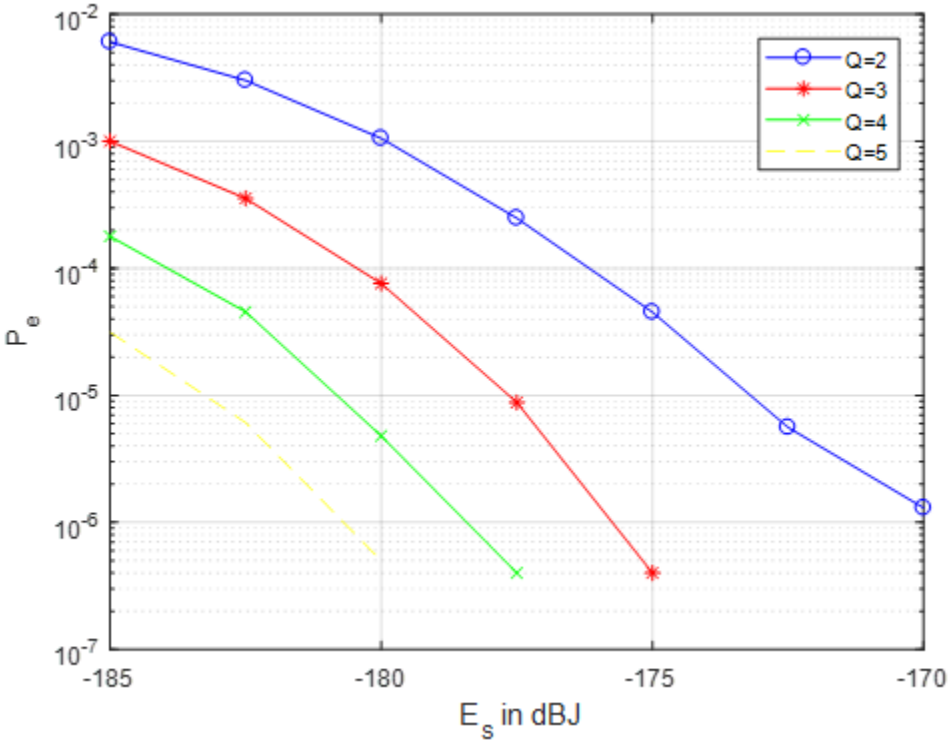

Figure 26 Performance of RC scheme for 2 apertures, 2-PPM and for different number of receivers Q

Fig. 27 represents the case of 4-PPM, 2 transmit apertures, and 2 receiver apertures system and Fig. 28 represents the case of 4-PPM, 3 transmit apertures and 3 receiver apertures system. In both scenarios, the results show that the ML method outperforms the EGC method. The BER performance of ML method starts at 0.007 in case of 2x2 system and starts at 0.002 in case of 3x3 system, however, the BER performance of the EGC method starts at 0.01 in case of 2x2 system and starts at 0.008 in case of the 3x3 system. This indicates that the level of improvement of the BER performance is greater in the ML method when there is an increase in the number of transmitter and receivers. In other words, the suboptimality of the simple EGC detection is more manifested for larger numbers of transmit apertures. Moreover, this result confirms that the ML decoder has a greater performance that than the EGC decoder but at the cost of higher complexity as discussed in sections 1.10 and 1.11.

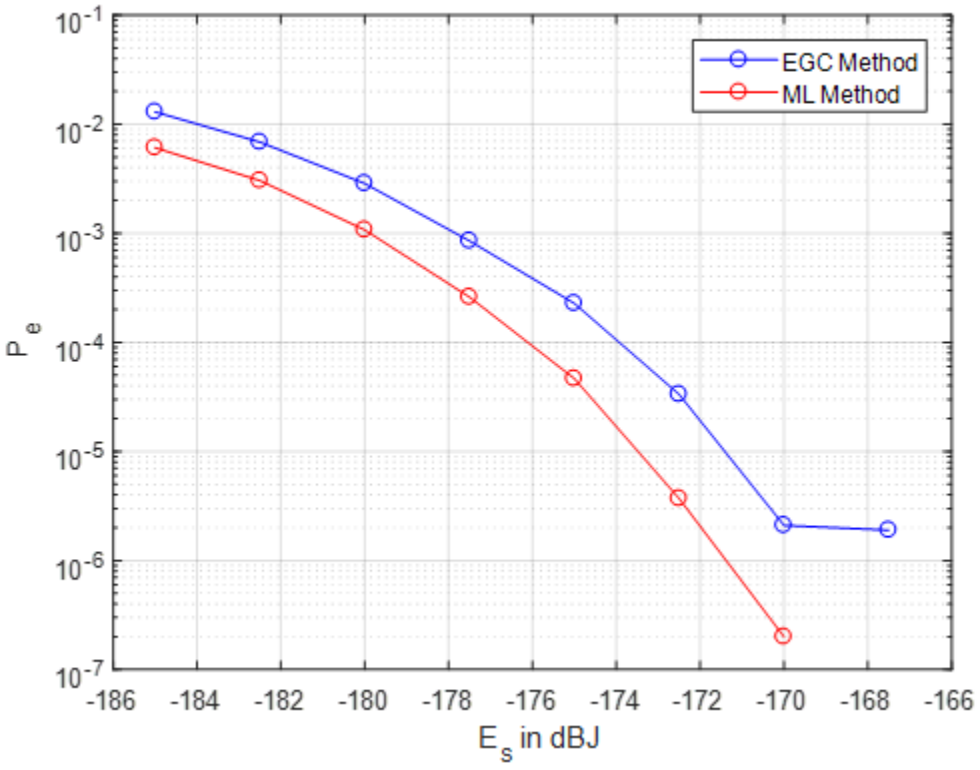

Figure 27 EGC versus ML for a 2X2 4-PPM RC scheme

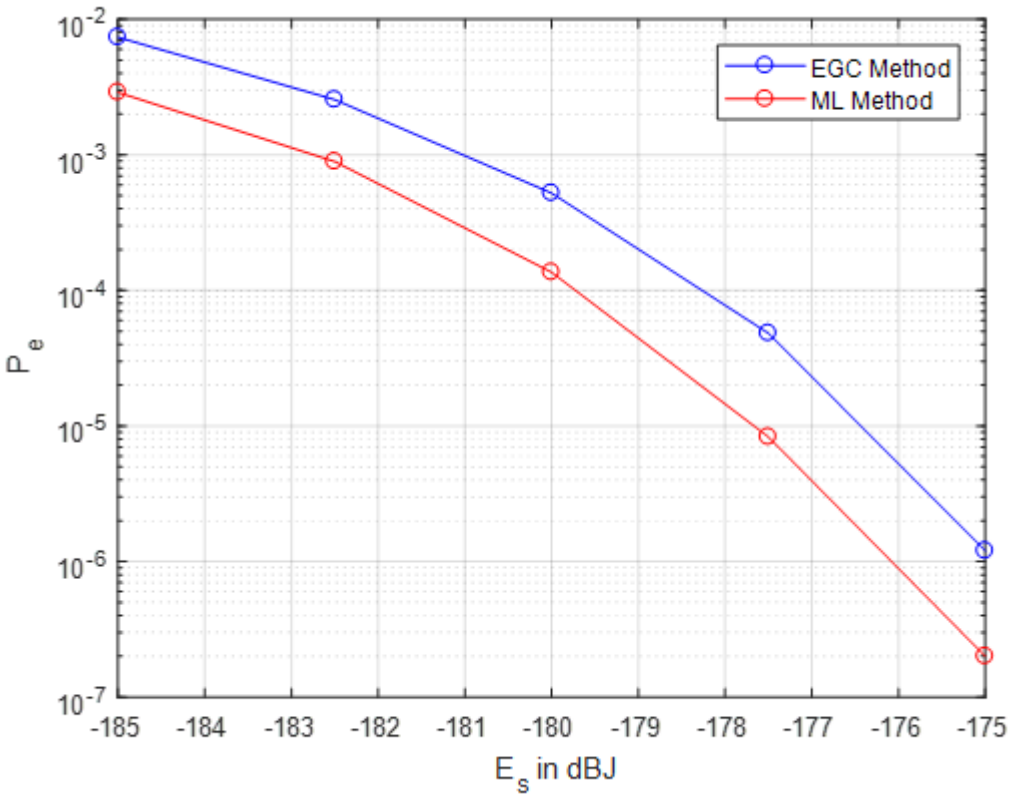

Figure 28 EGC versus ML for a 3X3 4-PPM RC scheme

Fig. 29 shows the OSM slot error, aperture error and total error obtained from both the numerical method and the theoretical method explained in section 3.4. We consider the case of 4x1 systems with 4-PPM.

Comparing both methods, the curves of all three errors are extremely close which means that the proposed theoretical method confirms on the results that were reached using the numerical method. The performance gap that can be observed for large of E_s, follows from the limitations of the Monte Carlo method where a very large number of channel realizations is required to produce reliable results in this energy region. Finally, results in Fig. 29 highlight the important fact that the apertures errors are much higher than the slot errors. In this context, the performance of OSM is dominated by the apertures errors and, hence, is limited by the capability of the OSM system in detecting the index of the pulsed transmit aperture.

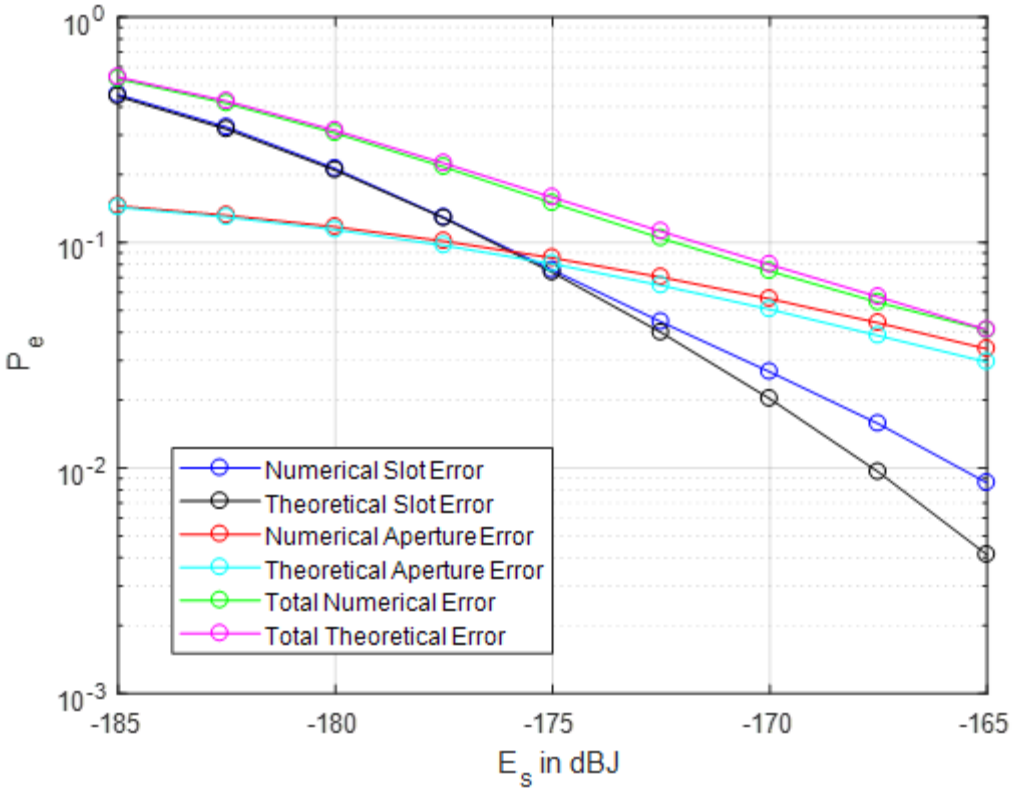

Figure 29 All errors of 4 x 1, 4-PPM OSM System

The same simulation setup of Fig. 29 is reproduced in Fig. 30 for 8x1 systems with 4-PPM. Again the accuracy of the theoretical analysis is demonstrated in this figure.

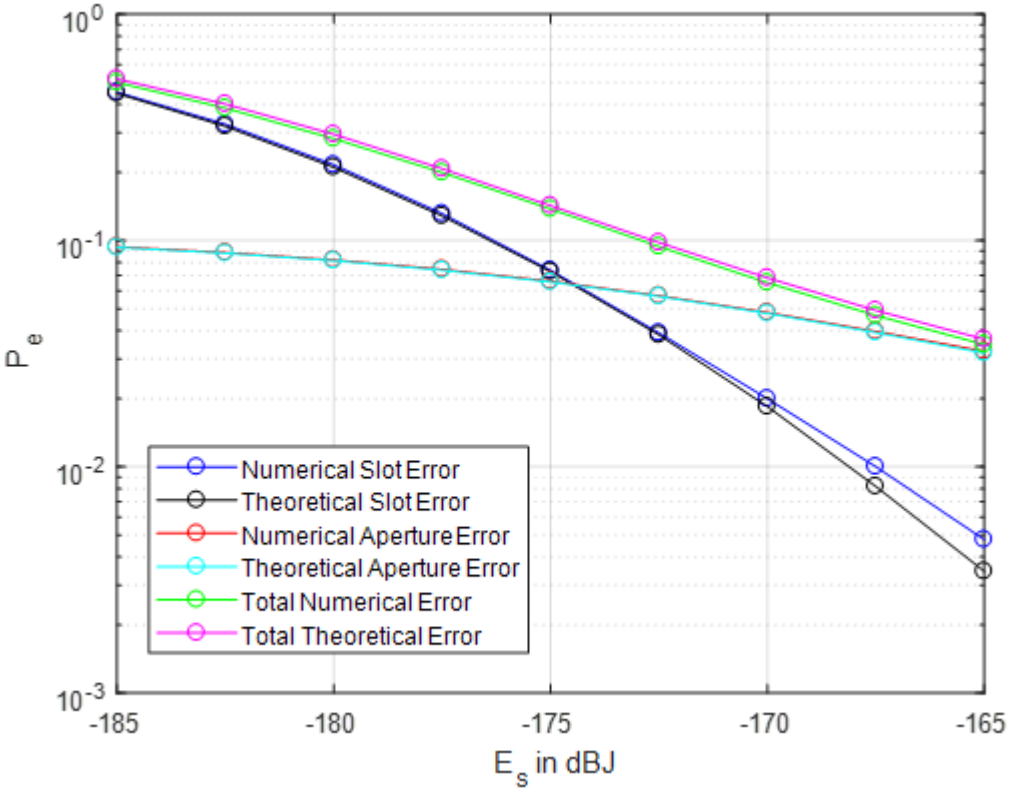

Figure 30 All errors of 8 x 1, 4-PPM OSM System

Fig. 31 and Fig. 32 show the performance of 2-PPM RC systems with 2x2 and 4x4 systems, respectively. Results show that the theoretical and numerical methods end up with almost the same results with higher accuracy especially in the lower optical signal power region.

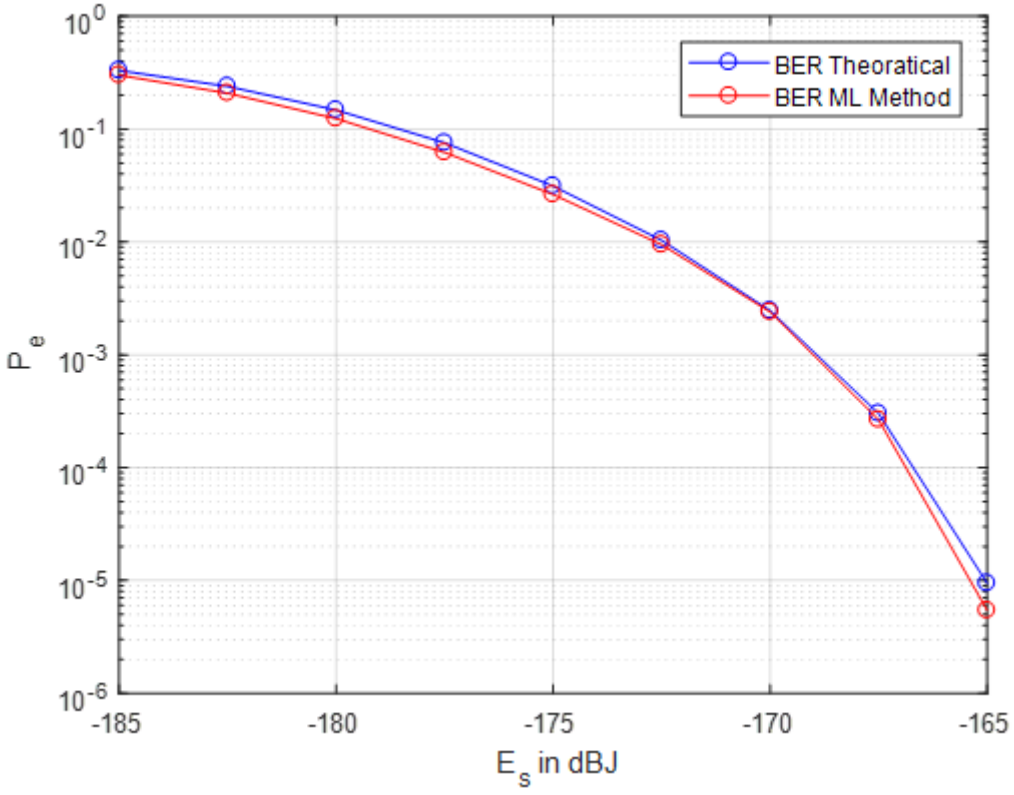

Figure 31 BER comparison between theoretical and numerical methods for 2x2 2-PPM RC scheme

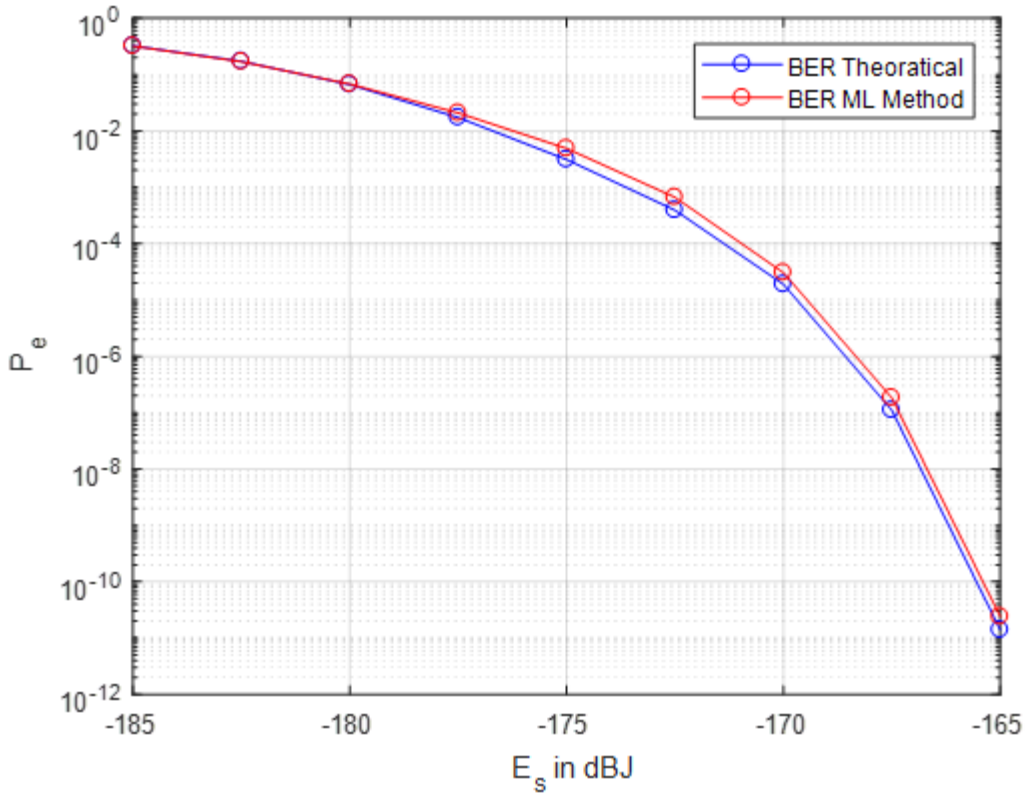

Figure 32 BER comparison between theoretical and numerical methods for 4x4 2-PPM RC scheme

Chapter 5

Conclusion & Future Work

We compared the three MIMO schemes that can be linked to IM/DD FSO systems; namely, the RC, OSM and SMux schemes. While the RC scheme is the most engaging regarding simplicity and performance, the SMux scheme has the dominating favorable position of accomplishing the highest bit rate making it an appropriate solution for high rate applications. In this case, despite the fact that the transmitted constellation has a cardinality of M^2 with M-PPM, the optimal 2x1 ML decoder can be executed with only three multiplications per symbol duration where it is passed judgment that these operations are unchallenging to implement in practical systems. Finally, OSM can be seen as a tradeoff between the RC and SMux schemes improving the rate compared to RC while loosening up some usage limitations with respect to SMux.

In this thesis, we proposed, modeled, and tested a novel theoretical method for calculating the SER of the RC and OSM schemes with a derived closed form-expression of the slot errors and aperture errors. This theoretical method showed exactly the same results as the numerical method. We analyzed the Poisson noise model in MIMO systems of all three schemes and the Matlab simulations. We compared the ML and EGC decoders in terms of performance and complexity and we found that the ML method has a higher performance in terms of SER. In addition to that, we have tested the 3 x Q SMux scheme where the simulations proved that this scheme results in higher rate which will be suitable for high data rate systems such as broadcasting but with substantial complexity.

Future work must target the ML decoder design of SMux systems with more than three transmit apertures. The theoretical SER of SMux needs to be evaluated in this general case as well.

References

[1] M.A. Khalighi, and M. Uysal, “Survey on Free Space Optical Communication: A Communication Theory Perspective “IEEE Communication Surveys & Tutorials, Vol. 16, No. 4, Fourth Quarter 2014

[2] G. J. Holzmann and B. Pehrson, The Early History of Data Networks (Perspectives). Hoboken, NJ, USA: Wiley, 1994.

[3] R.A. Alsemmeari, S. T.Bakhsh, and H.Alsemmeari, “Free-Space Optics Vs Radio Frequency Wireless Communication,” International Journal of Information Technology and Computer Science, vol. 8, no. 9, pp. 1–8, 2016.

[4] A. A. Huurdeman, The Worldwide History of Telecommunications. Hoboken, NJ, USA: Wiley-Interscience, 2003

[5] Z Ghassemlooy, W Popoola, and S Rajbhandari. Optical Wireless Communications: System and Channel Modelling with MATLAB{R}. Taylor & Francis, 2012.

[6] M. Groth, Photophones Revisited. [Online]. Available: http://www. bluehaze.com.au/modlight/GrothArticle1.htm

[7] J. Hecht, “Laser evolution,” SPIE Professional Magazine.

[8] F.E. Goodwin, "A Review of Operational Laser Communication Systems, "Proceedings of the IEEE, vol. 58, no. 10, pp. 1746–1752, 1970.

[9] J. Hecht and L. Long, Understanding fiber optics, vol. 3. Prentice Hall, 1993.

[10] H. A. Willebrand and B. S. Ghuman, "Fiber Optics Without fiber," IEEE Spectrum, vol. 38, no. 8, pp. 40–45, 2001

[11] M.M. Hassanand, G.Rather, “Scope of Potential In FSO Technology As Compared To RF Technology In The Next Generation Networks,” Journal of Network Communications and Emerging Technologies (JNCET) www. jncet.org, vol. 7, no. 9, 201

[12] A. Malik and P. Singh, "Free-Space Optics: Current Applications And Future Challenges," International Journal of Optics, vol. 2015, 2015.

[13] J. M. Kahn and J. R. Barry, “Wireless Infrared Communications,” Proc. IEEE, vol. 85, no. 2, pp. 265–298, Feb. 1997.

[14] S. Bloom, E. Korevaar, J. Schuster, and H. Willebrand, “Understanding The Performance Of Free-Space Optics,” J. Opt. Netw., vol. 2, no. 6, pp. 178–200, Jun. 2003.

[15] V. W. S. Chan, “Free-Space Optical Communications,” J. Lightw. Technol., vol. 24, no. 12, pp. 4750–4762, Dec. 2006.

[16] H. A. Willebrand and B. S. Ghuman, “Fiber Optics Without fiber,” IEEE Spectr., vol. 40, no. 8, pp. 41–45, Aug. 2001.

[17] E. Leitgeb et al., “Current Optical Technologies for Wireless Access,” in Proc. Int. ConTEL, Zagreb, Croatia, Jun. 2009, pp. 7–17.

[18] S. Vigneshwaran, I. Muthumani, and A. S. Raja, “Investigations on Free Space Optics Communication System,” in Information Communication and Embedded Systems (ICICES), 2013 International Conference on, pp. 819–824, IEEE, 2013.

[19] A. Mahdy and J. S. Deogun, “Wireless Optical Communications: A Survey,” in Wireless Communications and Networking Conference, 2004. WCNC. 2004 IEEE, vol. 4, pp. 2399–2404, IEEE, 200

[20] Abdulsalam Ghalib Alkholidi and Khaleel Saeed Altowij. Free Space Optical Communications Theory and Practices. page Ch. 0. In Tech, Rijeka, 2014

[21] C. Abou-Rjeily, “Diversity Orders and Coding Gains of Repetition Coding And Transmit Laser Selection Over MIMO Free-Space Optical Links,” in Wireless Communications Systems (ISWCS), 2014 11th International Symposium on, pp. 90–94, IEEE, 2014.

[22] E. SYSTEM, “EC SYSTEM Free Space Optics Equipment.” http://www.ecsystem.cz/en/products/free-space-optic-equipment.

[23] S. Patrick, “Why Hasn’t Free Space Optics Been Adopted for Communications On Earth?” https://www.quora.com/Why-hasnt-Free-Space-Optics-been-adopted-for-communications-onearth.

[24] I. K. Son and S. Mao, “A Survey of Free Space Optical Networks,” Digital communications and networks, vol. 3, no. 2, pp. 67–77, 2017.

[25] A. Malik and P. Singh, "Free-Space Optics: Current Applications And Future Challenges," International Journal of Optics, vol. 2015, 2015.

[26] S. Vigneshwaran, I. Muthumani, and A. S. Raja, “Investigations on Free Space Optics Communication System,” in Proceedings of the International Conference on Information Communication & Embedded Systems (ICICES '13), pp. 819–824, IEEE, Chennai, India, February 2013.

[27] H. A. Fadhil, A. Amphawan, H. A. B. Shamsuddin et al., “Optimization of Free Space Optics Parameters: An Optimum Solution for Bad Weather Conditions,” Optik, vol. 124, no. 19, pp. 3969–3973, 2013.

[28] http://www.laseroptronics.com/index.cfm/id/57-66.htm.

[29] A. K. Rahman, M. S. Anuar, S. A. Aljunid, and M. N. Junita, “Study of Rain Attenuation Consequence in Free Space Optic Transmission,” in Proceedings of the 2nd Malaysia Conference on Photonics Telecommunication Technologies (NCTT-MCP '08), pp. 64–70, IEEE, Putrajaya, Malaysia, August 2008.

[30] M. Ijaz, Z. Ghassemlooy, J. Pesek, O. Fiser, H. Le Minh, and E. Bentley, “Modeling of Fog And Smoke Attenuation In Free Space Optical Communications Link Under Controlled Laboratory Conditions,” Journal of Lightwave Technology, vol. 31, no. 11, Article ID 6497447, pp. 1720–1726, 2013.

[31] Z. Ghassemlooy, J. Perez, and E. Leitgeb, “On The Performance of FSO Communications Links Under Sandstorm Conditions,” in Proceedings of the 12th International Conference on Telecommunications (ConTEL '13), pp. 53–58, IEEE, Zagreb, Croatia, June 2013.

[32] K. Rammprasath and S. Prince, “Analyzing The Cloud Attenuation on the Performance of Free Space Optical Communication,” in Proceedings of the 2nd International Conference on Communication and Signal Processing (ICCSP '13), pp. 791–794, Melmaruvathur, India, April 2013

[33] S. A. Al-Gailani, A. B. Mohammad, R. Q. Shaddad, and M. Y. Jamaludin, "Single and Multiple Transceiver Simulation Modules For Free-Space Optical Channel In Tropical Malaysian Weather," in Proceedings of the IEEE Business Engineering and Industrial Applications Colloquium (BEIAC '13), pp. 613–616, Langkawi, Malaysia, April 2013.

[34] E. Zedini, H. Soury, and M.-S. Alouin, "On the Performance Analysis of Dual-Hop Mixed FSO/RF Systems," IEEE Transactions On Wireless Communications, Vol. 15, No. 5, May 2016.

[35] O.M.S. AI-Ebraheemy. M. Salhab, A. Chaaban, “Precise Outage Analysis of Mixed RF/Unified-FSO DF Relaying with HD and 2 IM-DD Channel Models” Department of Electrical Engineering, King Fahd University of Petroleum & Minerals, Dhahran 31261, Saudi Arabia §CEMSE Division, King Abdullah University of Science & Technology, Thuwal, Saudi Arabia

[36] Abou-Rjeily, C. (2014). All-Active and Selective FSO Relaying: Do We Need Inter-Relay Cooperation? Lightwave Technology, Journal of, 32(10), 1899-1906.

[37] V. Jamali, D. S. Michalopoulos, M. Uysal, and R. Schober, “Link Allocation for Multiuser Systems with Hybrid RF/FSO Backhaul: Delay-Limited and Delay-Tolerant Designs “IEEE Transactions On Wireless Communications, Vol. 15, No. 5, May 2016"

[38] G. T. Djordjevic, M. I. Petkovic, A. M. Cvetkovic and G. K. Karagiannidis, "Mixed RF/FSO Relaying with Outdated Channel State Information "IEEE Journal On Selected Areas in Communications, Vol. 33, No. 9, September 2015

[39] M. Safari, and M. Uysal, “Relay-Assisted Free-Space Optical Communication “IEEE Transactions On Wireless Communications, Vol. 7, No. 12, December 2008

[40] M. Safari and M. Uysal, “Do We Really Need Ostbcs for Free-Space Optical Communication with Direct Detection?” IEEE Trans. Wireless Commun., vol. 7, no. 11, pp. 4445 – 4448, Nov. 2008.

[41] C. Abou-Rjeily, “Performance Analysis of FSO Communications with Diversity Methods: Add More Relays or More Apertures?” IEEE J. Select. Areas Commun., vol. 33, no. 9, pp. 1890 – 1902, Sep. 2015.

[42] N. Letzepis and A. G. I. Fabregas, “Outage Probability of the Gaussian MIMO Free-Space Optical Channel with PPM,” IEEE Trans. Commun., vol. 57, no. 12, pp. 3682–3690, Dec. 2009.

[43] J. Zhang, L. Dai, Y. Han, Y. Zhang, and Z. Wang, “On The Ergodic Capacity of MIMO Free-Space Optical Systems Over Turbulence Channels,” IEEE J. Select. Areas Commun., vol. 33, no. 9, pp. 1925–1934, Sep.2015.

[44] S. G. Wilson, M. Brandt-Pearce, Q. Cao, and J. H. Leveque, “Free-Space Optical MIMO Transmission with Q-Ary PPM,” IEEE Trans. Commun., vol. 53, no. 8, pp. 1402–1412, Aug. 2005.

[45] S. G. Wilson, M. Brandt-Pearce, Q. Cao, and M. Baedke, “Optical Repetition MIMO Transmission with Multipulse PPM,” IEEE J. Select. Areas Commun., vol. 23, no. 9, pp. 1901–1910, September 2005.

[46] T. Ozbilgin and M. Koca, “Optical Spatial Modulation Over Atmospheric Turbulence Channels,” J. Lightwave Technol., vol. 33, no. 11, pp. 2313–2323, June 2015.

[47] A. Jaiswal, M. R. Bhatnagar, and V. K. Jain, “Performance Evaluation of Space Shift Keying in Free-Space Optical Communication,” IEEE J. Opt. Commun. Netw., vol. 9, no. 2, pp. 149–160, Feb. 2017.

[48] H. Nouri, F. Touati, and M. Uysal, “Diversity-Multiplexing Tradeoff for Log-Normal Fading Channels,” IEEE Trans. Commun., vol. 64, no. 7, pp. 3119–3129, July 2016.

[49] M. T. Dabiri, M. J. Saber, and S. M. S. Sadough, “On The Performance of Multiplexing FSO MIMO Links in Log-Normal Fading with Pointing Errors,” IEEE J. Opt. Commun. Netw., vol. 9, no. 11, pp. 974–983, Nov. 2017.

[50] G. Yang, M.-A. Khalighi, T. Virieux, S. Bourennane, and Z. Ghassemlooy, “Contrasting Space-Time Schemes for MIMO FSO Systems with Non-Coherent Modulation,” in IEEE Int. Workshop on Optical Wireless Commun., Oct 2012, pp. 1–3.

[51] N. Letzepis, K. D. Nguyen, A. G. I Fabregas, and W. G. Cowley, “Outage Analysis of the Hybrid Free-Space Optical and Radio-Frequency Channel,” IEEE J. Select. Areas Commun., vol. 27, no. 9, pp. 1709–1719, Dec.2009

[52] D. Cox. Cochannel interference considerations in frequency reuse small-coverage-area radio systems. IEEE Trans. Communications, 30(1):135–142, January 1982.

[53] Arun k. majumdar, "Advanced Free Space Optics (A System Approach)", New York: Springer Series in Optical Sciences, Vol.186, 2015.

[54] Z. Ghassemlooy, W. Popoola, and S. Rajbhandari, Optical Wireless Communications: System and Channel Modelling with MATLAB, New York: CRC Press, 2013

[55] I N Osahon, S Rajbhandari, and W O Popoola. Multi-layer perceptron as equalizers for multilevel pulse amplitude modulation scheme in SI-POF. In 2016 International Conference for Students on Applied Engineering (ICSAE), pages 318–322, Oct 2016

[56] S. G. Wilson, M. Brandt-Pearce, Q. L. Cao, and M. Baedke, “Optical Repetition MIMO Transmission with Multipulse PPM,” IEEE on Selected Areas in Communications, vol. 23, no. 9, pp. 1901– 1910, Sept. 2005.

[57] P. Deng, M. Kavehrad, Z. Liu, Z. Zhou, and X. Yuan, “Capacity of MIMO Free-Space Optical Communications Using Multiple Partially Coherent Beams Propagation Through Non-Kolmogorov Strong Turbulence,” Opt. Exp., vol. 21, no. 13, pp. 15 213–15 229, Jul. 2013.

[58] S.M. Alamouti, “A Simple Transmit Diversity Technique for Wireless Communications,” IEEE Journal on Selected Areas in Communications, vol. 16, no. 8, pp. 14511458, Oct 1998.

[59] M. K. Simon and V. A. Vilnrotter, “Alamouti-Type Space-Time Coding for Free-Space Optical Communication with Direct Detection,” IEEE Transactions on Wireless Communications, vol. 4, no. 1, pp.

[60] A. Garcia-Zambrana, “Error Rate Performance for STBC in Free-Space Optical Communications Through Strong Atmospheric Turbulence,” IEEE Communications Letters, vol. 11, no. 5, pp. 390–392, May 2007.

[61] R. Mesleh, H. Elgala, and H. Haas, “Optical Spatial Modulation,” IEEE/OSA Journal of Optical Communications and Networking, vol. 3, no. 3, pp. 234–244, Mar. 2011

[62] E. Bayaki and R. Schober, “On Space-Time Coding for Free-Space Optical Systems,” IEEE Transactions on Communications, vol. 58, no. 1, pp. 58–62, Jan. 2010.

[63] M. D. Renzo, H. Haas, and P. M. Grant, “Spatial Modulation for Multiple-Antenna Wireless Systems: A Survey,” IEEE Communications Magazine, vol. 49, no. 12, pp. 182–191, Dec. 2011

[64] J. Jeganathan, A. Ghrayeb, and L. Szczecinski, “Spatial Modulation: Optimal Detection and Performance Analysis,” IEEE Communications Letters, vol. 12, no. 8, pp. 545–547, 2008

[65] Ankit Garg, Manav R. Bhatnagar, Olivier Berder, Baptiste Vrigneau. Improved beamforming for FSO MISO system over gamma-gamma fading with pointing errors. IEEE Advanced Technologies for Communications, Oct 2016, Hanoi, Vietnam. Advanced Technologies for Communications (ATC), 2016 International Conference on, pp.362-368

[66] P. K. Sharma, A. Bansal and M. R. Bhatnagar, "Arbitrary Beamforming Based FSO MIMO System in Atmospheric Turbulence and Misalignment Errors," 2016 Twenty-Second National Conference on Communication (NCC), Guwahati, 2016, pp. 1-5